*J. Fluid Mech.* (1984), *vol.* 142, *pp.* 309–342
*Printed in Great Britain*



# Analysis of the forced ventilation in containership holds

By HOWARD R. BAUM AND JOHN A. ROCKETT

Center for Fire Research, National Engineering Laboratory, National Bureau of Standards, Washington, DC 20234

(Received 2 September 1983)

An analysis of the fluid flow and mass transfer induced by ventilation systems in containership holds was carried out. The result of the work was used to support the U.S. position before a committee of the International Convention on Safety to Life at Sea. The analysis consists of a detailed calculation of the forced motion through an interconnected set of narrow, stably stratified, vertical air passages, which represent an idealized containership hold. The results of this calculation were then used to predict the vapour concentration of spilled volatile material assumed to lie at the bottom of the vertical air passages. The result is a set of formulae which determine the rate of extraction of volatile material as a function of hold geometry, ventilation parameters, and ambient stratification. A variety of computed results are presented. The results indicate the crucial importance of locating the extractor as close to the hold bottom as technically possible.

## 1. Introduction

The purpose of this study was to obtain the information necessary to prepare a quantitative statement on the degree of fire hazard that might exist in the hold of a large containership as a function of the amount and nature of the hold ventilation and amount and kind of leakage of flammable liquid or gas cargo. The effort was mainly analytic, although some sea tests were conducted by Sealand Corporation to determine the degree to which the thermal conditions assumed by the analysis were found in practice.

Containerships play a major role in the U.S. Merchant Marine. The majority of the non-bulk seagoing cargo into and out of the U.S. is now moved in containers. Some of this cargo is classified as 'dangerous cargo', such as flammable liquids and gases, and are regulated in treaty provisions based on recommendations of the International Maritime Consultative Organization (IMCO).

Under existing regulations stowage limitations, resulting from the types and amounts of cargo classed as dangerous, reduce shipment-scheduling flexibility. IMCO has considered new regulations which would somewhat relax the dangerous category definitions for ships with adequate hold ventilation or detection and inerting systems. The basis for their action is the belief, by some members of the committee, that ventilation would keep the concentration of leaking and vaporizing flammable gas below the flammable or explosive limit. However, prior to this study, there did not appear to be a rational basis for establishing a suitable rate of ventilation. A study on the scale of this one could not address the full range of situations that might arise, but the most prevalent situation was considered. Using the results of this study, a position was developed and presented by the U.S. representative to IMCO as a

counter to the *ad hoc* opinions originally put forward by others. After discussion, a position close to the U.S. position was adopted by the committee.

Container-freight forwarding is a highly automated process using ships often specifically built for container freight and complex dockside equipment matched to the ship design. Containers of a uniform size are closely stacked within the holds, filling all the space available after allowance for structure, container guides and spaces at the sides, especially near the ends of the ship, due to the non-rectangular shape of holds. Current practice loads a hold to its maximum capacity. In the centre portion of a ship, with wing tanks occupying the space between the hull plating and the side combing of the hatch, the only significant voids would be between the top of the containers and the underside of the hatch covers; and at one end of the container stacks, where deep framing of the transverse bulkhead result in a array of rectangular spaces interconnected by lightening holes in the frames. The spaces between stacks of containers, between the containers and the wing-tank walls, or between the end of the container stacks and the smooth (non-framed) side of a transverse bulkhead would be only that needed for the container guides, typically about 10 cm between stacks of containers and half this between the containers and bulkhead (see figure 1). On some ships there may be fixed, heavy longitudinal beams to support the hatch cover. The gaps between container stacks on either side of such a beam would be somewhat wider. Where wing tanks are not used and at the ends of the ship, a fairly large void will exist between the hull plating and the outermost container stack. This will be partially subdivided by the transverse and longitudinal framing. The container stacks rest on the flat, smooth double bottom tank top. Although an air space some 10 cm deep exists under the containers, this is cut off from the inter-container gaps and end void by side- and endrails or skirts of the container so that effective communication with this space is limited by the thickness of the corner pads of the containers, a gap perhaps less than 2 cm. Should a liquid be spilled on the tank top, it would be able to flow under the containers as the ship rolled, but liquid evaporated under the containers would not easily escape to the rest of the hold.

The accident scenario envisaged involves a container carrying general cargo including some flammable liquid in cans or drums. For any of a number of reasons – a defective drum, inadequate dunnage and securing, rough handling of the container, etc. – flammable liquid is assumed to escape into the interior of the container. Although a container in good condition is quite weathertight, an older container, especially if it has been roughly treated (a situation likely to accompany disruption of its cargo), may allow a liquid spilled inside, to leak out. It is assumed that liquid does escape and flows down over the outside of the containers below to the bottom of the hold, where it accumulates in a puddle, which is spread by rolling and pitching of the ship to wet the entire bottom of the compartment. In the case considered for the numerical examples used throughout this paper, the liquid is heptane and the tank top area is 324 m$^2$. If 208 litres (55 U.S. gallons) of liquid reached the bottom of the hold and spread uniformly over the tank top, the liquid layer would be only $\frac{2}{3}$ mm thick.

Consider the implications of this accident first as it affects conditions inside the container and next as it affects conditions in the hold. Inside the container the air will be essentially stagnant for any plausible hold ventilation scheme. Accumulated liquid will evaporate, reaching a local equilibrium conentration depending on the container temperature. Hold temperatures measured by Sealand on a run from Houston to Rotterdam (von Iperen 1979) in the fall of 1978 ranged from 10–28 °C (50–83 °F). From figure 2 (Hodgman 1943) it is seen that the equilibrium vapour

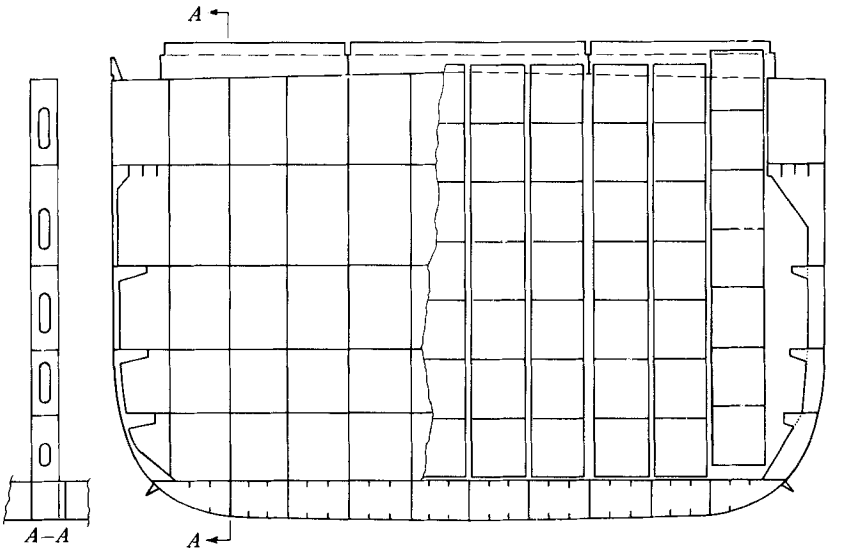


FIGURE 1. Cross-section of a typical containership near its midsection. To the right is shown the container stacking and to the left the bulkhead framing.

pressure of heptane, for these temperatures, ranges from 20–53 mmHg, yielding corresponding volume concentrations of 2.6–7.0 %. Lewis & von Elbe (1961) give the flammability limits for heptane in air as 1.2 and 6.7 %. Thus the undiluted heptane vapours will lie within the flammable limits throughout the expected temperature range. Heptane ($C_7H_{16}$) vapours are heavier than air. The mean molecular weight at standard temperature and pressures of the equilibrium heptane–air mixture for this range of vapor pressures is 30.84–34.11, compared with 28.97 for air. This will tend to inhibit mixing of the heavy vapours with the rest of this air in the container, but, over a long period of time, through diffusion, a substantial volume of combustible vapour could accumulate inside the container (121–312 g of heptane/m$^3$ of air in a container with total volume about 90 m$^3$ and void volume estimated at 10 m$^3$). Our accident scenario supposed that the container would allow the spilled liquid to leak out, but, of course, it might not, or might leak very slowly. Thus, if an ignition source of sufficient strength to ignite the vapours were found within the container, a vapour deflagration could occur, followed by fire. Recall that this situation is independent of the amount and type of hold ventilation and that, for the chemical and temperatures chosen, there is little possibility of escaping danger by exceeding the rich flammable limit after a long time.

If the container leaks, some or most of the liquid can escape, possibly alleviating the hazard just described, but creating another in the ship's hold. As already noted, the liquid will form a thin but extensive puddle on the tank top. If there is a low-point sump in the hold, a substantial amount of the spill may drain into it and could be pumped to a safe holding tank. Such an arrangement seems the most suitable way to remove any substantial amount of liquid. However, evaporation will occur in the hold just as it does in the container, but, in the hold, ventilation can greatly reduce the hazard.

Consider first the zero-ventilation situation in an unstratified hold. While, as just discussed, there might be 1–3 kg of fuel vapour in the container where the spill originated, the ship's hold is so large that, for a plausible spill volume, evaporation

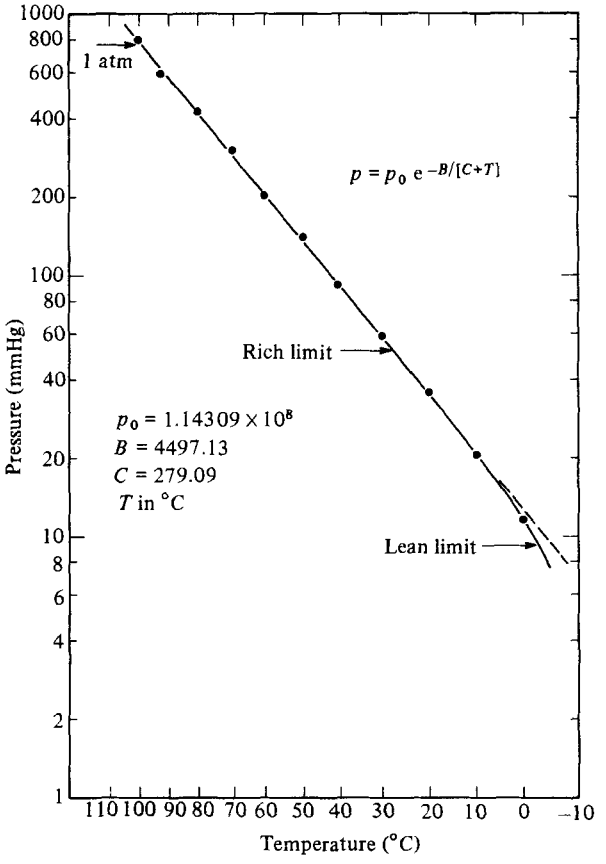


FIGURE 2. Vapour pressure versus temperature for heptane. Rich and lean limits are for an air environment.

followed by thorough mixing might exhaust the available vapour before the lean-limit concentrations were reached. For a hypothetical ship with wing tanks, i.e. minimal side voids, loaded with 10 rows of 35 ft containers across the hold each row 7 containers high, the total hold volume might be about 6500 $m^3$ (230000 $ft^3$) and the void volume 1760 $m^3$ (62000 $ft^3$). This void volume could carry, for the range of temperatures expected, from 210–550 kg heptane, or approximately the contents of $1\frac{1}{3}$–$3\frac{1}{2}$ 55 gallon drums. A very large ship without wing tanks would have considerably more void volume in its midships holds while, in the ends a ship, there could be considerably less void volume. In any event, the advantage of a low-point sump becomes clearer in this context since it could remove much of the spill liquid before it evaporated. As noted earlier, the film of liquid from a 55 gallon spill, spread evenly over the tank top of a large ship is quite thin. Since some residual film, puddles in irregular low spots, etc., must be anticipated, there would be a significant reservoir for evaporation even with an efficient sump. This residual volume is difficult to estimate, but for a low-viscosity liquid might be about 20–30 gallons in so large a space. For the void volume of our example (1760 $m^3$) at the lean-limit concentration there would be 94 kg of heptane vapour or the result of evaporating 33 gallons. Thus, by using a sump, there is the possibility of keeping the average composition of the vapour below the flammable limit.

Although the average composition of the vapour might be kept below the flammable limits, during the evaporation process (while liquid remains) there will be a region near the liquid surface in which the vapour concentration will approach the equilibrium vapour concentration corresponding to the liquid temperature. As we have seen, this can be expected to be well within the flammable limits. The purpose of ventilation is to keep the volume of gas that is within the flammable limits as small as possible. If the air in the hold were continually stirred, for example by natural convection created by an unstable vertical temperature gradient – bottom of the hold warmer than the top – the same situation described under zero ventilation would apply. However, an unstable temperature gradient was observed only intermittently on the instrumented containership run from Houston to Rotterdam, and then only in the upper portion of the hold. The lowest thermocouple was always the coolest. Throughout most of the voyage the hold air was stably stratified for all heights measured. In addition to the temperature stratification, if there are pools of flammable liquid at the bottom of the hold, the vapour just above these pools will be heavier than pure air. This may be expressed as an added equivalent thermal stratification by giving the temperature difference required to produce the same density difference in pure air as is produced by the fuel vapour. For heptane at the temperature observed, this ranges from about 20–50 °C. By contrast the true thermal stratification on the instrumented sea run never exceeded 3 °C, and was more typically less than 1 °C. Thus the combination of a stable temperature field and heavy evaporated liquid vapour tends to be extremely stable near the tank top (hold bottom) and generally stable, though much less so, elsewhere.

If there were a transverse temperature difference, one side of the hold warmer than the other, a circulation would develop (Turner 1973; Birikh *et al.* 1969). In an empty hold a narrow boundary-layer flow would move up the warmer side across the top of the hold and down the cooler side. Near-stagnant conditions would be found in the interior of the hold. The flow across the tank top would also be confined to a thin boundary layer. In a loaded ship, owing to the presence of the container stacks, this flow would be strongly inhibited except in the end void associated with the bulkhead framing, and there the framing would considerably reduce the general flow. In practice, the flow induced by a transverse temperature gradient in the presence of a stable vertical gradient would probably only be significant in the two side voids of a ship without wing tanks. The circulation would be between the sides of the ship and the outer side of the outermost container stacks. Such flow has not been considered in this study.

The flow that seems most likely to affect the vapour bubble over evaporating liquid on the tank top is that associated with forced ventilation. Obviously, for the well-mixed case (unstable stratification) the location of the suction and inlet for the forced flow are relatively unimportant, although they should be well separated. In the stably stratified case this is not true. Both since the stable case is more prevalent and since, in the unstable case, the suction may be located anywhere and might as well be placed advantageously for the stable situation, the stable case has been given priority in our study. With stable stratification and flammable vapours heavier than air originating from a liquid spill, the suction should be close to the bottom of the hold and the inlet placed well above it. As will be discussed in detail in the following sections, the air flow will at first spread laterally from the inlet with very limited vertical movement. There will be a relatively slow drift downward to the level of the suction, followed by lateral movement in the plane of the suction, again with little vertical motion, to the suction location. If the suction is located above the tank top (at the bottom

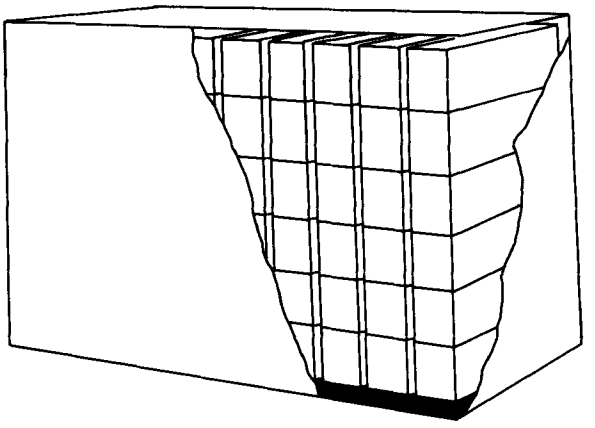

FIGURE 3. Idealized containership hold loaded with containers.

of the hold shown in figure 1) the gas below the suction will tend to be stagnant. In the stably stratified case, vertical movement of the gas is facilitated where it can exchange heat with its surroundings. The result is that the vertical drift from the level of the inlet to that of the suction is not uniform but concentrated in thin boundary layers adjacent to the container stacks and ship structure. The more stable the stratification the narrower these boundary layers become. For the geometry and temperature differences found in a typical containership these boundary layers are only a few centimetres thick. The result is that virtually the same flow can move down the 10 cm wide gap between container stacks as down the several-metre wide gap between the outermost container stack and the side of the ship. Only when the gap is narrower than the combined thickness of the two boundary layers is the flow decreased. This may occur in the gap between the end of the container stacks and the smooth side of the bulkhead.

In all the above, the accident was assumed to involve a liquid spill. Although this appears to be the most likely type of accident, some materials could be released whose vapours are lighter than air. To deal with this eventuality, it has been proposed that the forced ventilation inlet be located near but not at the top of the hold and that a suction pulling a minor fraction of the ventilation be provided at the highest point in the hold, just under the hatch cover.

## 2. Basic assumptions of the theoretical model

In order to develop a quantitative model, it is necessary to know the geometry and thermal stratification of a typical containership hold. The most obvious feature of such holds (on efficiently designed ships) is that most of the available space is occupied by containers. The only air spaces are narrow vertical slots between stacks of containers, similar but less narrow voids at ends and/or sides of the stacks, and a gap between the top of the container stacks and the hatches. The size and shape of these vary from ship to ship, and from one hold to the next on a given ship. The temperature distribution in each hold is dependent on both the ship and its thermal environment over a period of time. In general, the environment is highly dependent on the ship's route and both seasonal and daily weather patterns. The conditions prevailing in tanks adjacent to the hold are also important and may vary markedly

during a voyage. Given this environment, the complete determination of the thermal balance on a ship is itself a formidable task.

Rather than attempt to model the detailed features of a single hold and thermal environment, a set of simplifying assumptions is introduced, which permits the analysis to be reduced to a tractable size and scope, and still retain some dependence on the physical and geometric parameters described above. These assumptions are as follows:

(1) The hold is rectangular. The air spaces consist of narrow rectangular vertical slots separating container stacks and a narrow rectangular vertical void at one end of the hold. The idealized hold is shown schematically in figure 3.

(2) The temperature distribution in the hold is stably stratified and varies linearly from top to bottom. The containers and ship hull are in thermal equilibrium with this distribution. Thus all motions are due to ventilation.

(3) The ventilation system is designed so that air enters at the top of the hold and exits in the end void. The overall air volume flow is consistent with creeping motion (inertia forces unimportant).

Finally, in order to estimate the rate at which spilled material is picked up it is necessary to impose a spill scenario on the model. It is assumed that the spill material collects at the bottom of the slots between container stacks. The material is picked up as vapour in a concentration boundary layer formed at the bottom of the slot. All material caught up in this boundary layer is assumed to exit with the ventilation air. The analysis then proceeds as follows.

First the conditions for low-Reynolds-number flow are established and the small-scale motion in a single slot is determined. This leads to an equation for the pressure that governs the large-scale motion in a single slot. This equation is then solved assuming that the pressure in the end void where the flow exits is known. The next step is the solution for the pressure in the end void, which ties together the large-scale motion in the entire hold. Then the local flow in the bottom of each slot is obtained. The final step is the calculation of the concentration boundary layer in the slot bottom, which determines the actual pickup of spill material.

## 3. Slot flow in a stably stratified environment

As mentioned above, the volume available for air movement in a containership hold may be usefully idealized as a collection of narrow vertical and horizontal slots. The analysis of the motion in a single slot is thus a necessary precondition for a study of the air movement throughout the hold. In order to proceed, we must first establish that the creeping-flow regime is encountered for realistic values of the governing flow parameters. Then approximate solutions to the equations of motion valid in the appropriate flow regime can be constructed. Finally these solutions will be related to the large-scale motion in the hold.

Consider a vertically oriented slot of width $2d$, height $h$ and length $l$ (figure 4). The equations governing the steady motion of a viscous incompressible fluid affected by buoyancy forces can be written in the Boussinesq approximation as

$$\nabla \cdot \boldsymbol{u} = 0, \tag{1a}$$

$$(\boldsymbol{u} \cdot \nabla)\,\boldsymbol{u} + \frac{1}{\rho}\nabla p^* + \frac{T - T_0}{T_0}\boldsymbol{g} = \nu \Delta \boldsymbol{u}, \tag{1b}$$

$$(\boldsymbol{u} \cdot \nabla)\,T = \frac{\nu}{Pr}\Delta T. \tag{1c}$$

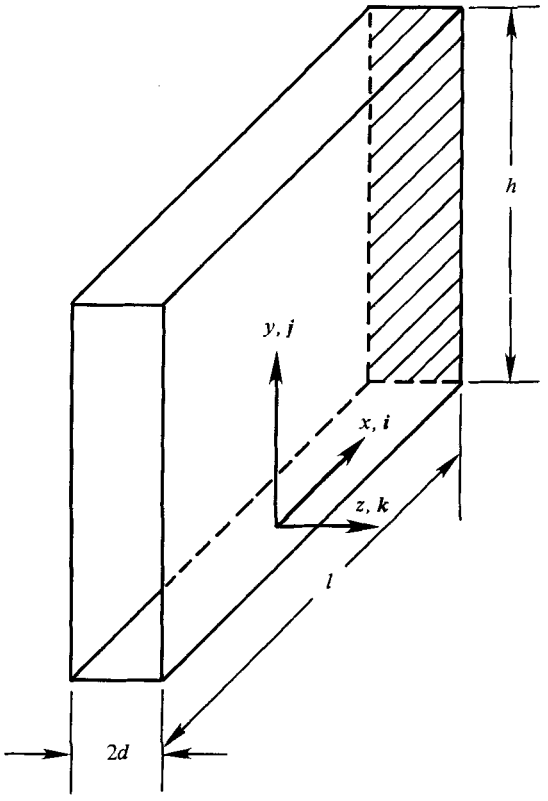


FIGURE 4. Geometry of the space between two stacks of containers (inter-container slot).

Here $\boldsymbol{u}$ is the velocity vector, $p^*$ the pressure and $T$ the temperature in the fluid. The density $\rho$, kinematic viscosity $\nu$ and Prandtl number $Pr$ are properties of the fluid taken as constant corresponding to the hold bottom temperature $T_0$. The gravitational acceleration $\boldsymbol{g}$ is directed vertically downward, while $\nabla$ and $\Delta$ are respectively the gradient and Laplacian operators.

Equations (1$a$,$b$,$c$) represent the conservation of mass, momentum and energy respectively. It is anticipated that the ventilation system will be designed to induce mean (mass-averaged) velocities in the slot whose order of magnitude is such that air actually in the hold bottom can be swept out several times per hour. Let $m$ be the number of times per hour that a slot is swept out horizontally. Then a typical horizontal velocity must be of order $ml/\tau$, where $\tau$ is the period (one hour). The inertial terms (the nonlinear terms) in the horizontal momentum balance are then of order $(ml/\tau)^2/l$, while the viscous terms are of order $\nu(ml/\tau)/d^2$. The ratio of these two terms indicates the relative importance of viscous and inertial effects. It will be called the 'effective Reynolds number' in this report to distinguish it from more conventionally defined Reynolds numbers. This effective Reynolds number $Re$ for horizontal motion in the slot, which determines the flow regime of interest, is given by

$$Re = \frac{md^2}{\nu\tau}.$$

For slot widths and sweep and rates of interest the effective Reynolds number $Re$ is typically in the range $1 \leqslant Re \leqslant 10$.

For this range of values, the horizontal flow is effectively one in which the pressure forces balance the viscous forces on the fluid, as in pipe flow and in bearing lubrication (Schlichting 1955; Batchelor 1967). This occurs because the slot is so narrow in comparison with its length ($d/l \ll 1$) that velocities perpendicular to the plane of the slot (i.e. in the $z$-direction, see figure 4) are negligibly small compared with those in the plane of the slot. Although the above argument strictly applies to horizontal motions, it will be shown in detail below that the effect of stable stratification will be to reduce even further the importance of inertial effects on the fluid motion.

We now turn to a detailed study of the motion in the slot. Let $P_0$ and $T_0$ be reference values of the pressure and temperature of the air in the slot. The fluid velocity $\boldsymbol{u}$ may be expressed in component form (see figure 4) as

$$\boldsymbol{u} = u\boldsymbol{i}+v\boldsymbol{j}+w\boldsymbol{k}.$$

The dependent variables describing the state of motion may be represented as follows:

$$p^* = p_0-\rho g y+\rho\frac{T_1-T_0}{T_0}\frac{gh}{2}\left(\frac{y}{h}\right)^2+p\left(\frac{x}{l},\frac{y}{h}\right), \tag{2a}$$

$$T = T_0+(T_1-T_0)\frac{y}{h}+\theta\left(\frac{x}{l},\frac{y}{h},\frac{z}{d}\right), \tag{2b}$$

$$u = u\left(\frac{x}{l},\frac{y}{h},\frac{z}{d}\right), \quad v = v\left(\frac{x}{l},\frac{y}{h},\frac{z}{d}\right), \quad w = w\left(\frac{x}{l},\frac{y}{h},\frac{z}{d}\right). \tag{2c,d,e}$$

Here $g$ is the magnitude of the gravitational acceleration and $p$ is the dynamical part of the pressure. The remaining terms in the expression for $p^*$ are the hydrostatic values of the pressure. The term linear in $y/h$ in the expression for the temperature is the ambient stratification of the hold. This stratification is assumed to vary linearly between the upper temperature $T_1$ and $T_0$, where $T_1 > T_0$. The velocity component $w$ normal to the plane of the slot is smaller than the inplane components $u$ and $v$ by a factor $d/l$ or $d/h$. The conservation of momentum in the $z$-direction immediately leads to the conclusion that the dynamic pressure $p$ must be nearly independent of $z$.

It is convenient to work with non-dimensional variables defined as follows:

$$p = Re\,\rho g h\frac{T_1-T_0}{T_0}\hat{p}(\xi,\eta), \quad v = Re\,g d\frac{T_1-T_0}{T_0}\hat{v}(\xi,\eta,\zeta), \tag{3a,b}$$

$$\theta = Re\,(T_1-T_0)\hat{\theta}(\xi,\eta,\zeta), \quad \xi = \frac{x}{l}, \quad \eta = \frac{y}{h}, \quad \zeta = \frac{z}{d}. \tag{3c,d,e,f}$$

Substitution of the non-dimensional variables defined in (3) into the vertical momentum- and energy-conservation equations and neglecting terms of order $(d/h)^2$, $(d/l)^2$ or $Re$ yields

$$\frac{\partial\hat{p}}{\partial\eta}-\hat{\theta} = G^{-\frac{1}{2}}\frac{\partial^2\hat{v}}{\partial\zeta^2}, \quad \hat{v} = \frac{G^{-\frac{1}{2}}}{Pr}\frac{h}{d}\frac{\partial^2\theta}{\partial\zeta^2}, \quad G = \frac{T_1-T_0}{T_0}\frac{gd^3}{\nu^2}. \tag{4a,b,c}$$

The dimensionless parameter $G$, the Grashof number, is the fundamental parameter controlling the nature of the vertical motion in the slot. Its influence will be discussed in detail below.

Since $p(\xi,\eta)$ is independent of $\zeta$, (4) can be solved for the dimensionless vertical

velocity $v$ and temperature perturbation $\hat{\theta}$ as functions of the vertical pressure gradient $\partial p/\partial \eta$. The boundary conditions associated with (4) are

$$\hat{v}(-1) = \hat{v}(1) = 0, \quad \hat{\theta}(-1) = \hat{\theta}(1) = 0. \tag{5a,b}$$

The physical meaning of (5) is that the vertical velocity and temperature perturbation must vanish at the sides of the slot. The first boundary condition follows from the no-slip condition. The second comes from the assumption that the ambient stratification in the slot is controlled by the temperature distribution in the containers, which varies linearly with height.

The solution to (4) and (5) is given by

$$\hat{v} = \frac{\partial \hat{p}}{\partial \eta}\left(\frac{h}{d\,Pr}\right)^{\frac{1}{2}} \{a(\omega)\cos\omega\zeta\cosh\omega\zeta - b(\omega)\sin\omega\zeta\sinh\omega\zeta\}, \tag{6a}$$

$$\hat{\theta} = \frac{\partial \hat{p}}{\partial \eta}\{1 + a(\omega)\sin\omega\zeta\sinh\omega\zeta + b(\omega)\cos\omega\zeta\cosh\omega\zeta\}, \tag{6b}$$

$$a(\omega) = -\frac{\sin\omega\sinh\omega}{-\sin^2\omega + \cosh^2\omega}, \quad b(\omega) = -\frac{\cosh\omega\cos\omega}{-\sin^2\omega + \cosh^2\omega}, \quad \omega = \frac{1}{\sqrt{2}}\left(\frac{GPr\,d}{h}\right)^{\frac{1}{4}}. \tag{6c,d,e}$$

It should be noted that the above solution, while approximate in terms of the overall problem of interest, is in fact an exact solution of the equations of hydrodynamics for an infinitely long slot. This buoyancy layer was first found by Prandtl (1952) and by Gill (1966), and used by Gill in his analysis of thermally driven slot convection. Gill's analysis has been experimentally verified by Elder (1965). In the present application, the solution corresponds to a forced stratified channel flow. In the limit of zero stratification

$$\hat{v} = -\frac{\partial \hat{p}}{\partial \eta}\left(\frac{h}{d\,Pr}\right)^{\frac{1}{2}} \omega^2(1-\zeta^2). \tag{7}$$

Returning to dimensional variables, (7) can be rewritten in the classical form

$$v = -\frac{1}{2}\frac{d^2}{\mu}\frac{\partial p}{\partial y}\left[1 - \left(\frac{z}{d}\right)^2\right], \quad u = -\frac{1}{2}\frac{d^2}{\mu}\frac{\partial p}{\partial x}\left[1 - \left(\frac{z}{d}\right)^2\right]. \tag{8a,b}$$

Here $\mu$ is the viscosity of the air, and the solution for $u$ has been added. For large stratification, $\omega$ is not small. As an example, for a stable stratification $T_1 - T_0$ of 3 °C, with the reference temperature $T_0 = 300$ K and a slot half-width of 10 cm and width-to-height ratio $d/h = 0.01$, $\omega = 5.3$. For values of $\omega > 3$, (6) simplifies to the form

$$\hat{v} = -\frac{\partial \hat{p}}{\partial \eta}\left(\frac{h}{d\,Pr}\right)^{\frac{1}{2}} \{e^{-\omega(1-\zeta)}\sin[\omega(1-\zeta)] + e^{-\omega(1+\zeta)}\sin[\omega(1+\zeta)]\}. \tag{9}$$

Equation (9) represents a vertical flow that has effectively ceased except for a boundary layer of thickness $\omega^{-1}$ near each wall of the slot. Thus, for a given pressure gradient, there is much less vertical flow in the presence of stratification than in its absence. This can be seen more dramatically by calculating the vertical volume flux of air per unit of length. The vertical flux in dimensional variables is given by

$$\int_{-d}^{d} v\,dz = \frac{2d^3}{3\mu}\frac{\partial p}{\partial y} f(\omega), \quad f(\omega) = \frac{3}{8\omega^3}\frac{\sinh 2\omega - \sin 2\omega}{-\sin^2\omega + \cosh^2\omega}. \tag{10a,b}$$

| $\omega$ | $f(\omega)$ | $\omega$ | $f(\omega)$ |
|---|---|---|---|
| 0 | 1 | 3 | 0.0276 |
| 1 | 0.3299 | 4 | 0.0117 |
| 2 | 0.0878 | 5 | 0.0060 |

TABLE 1. Vertical pressure-gradient effectiveness $f(\omega)$ dependence upon stratification parameter $\omega$ defined in (10). $f(\omega)$ is the ratio of vertical to horizontal flow capable of being produced by a given pressure gradient.

This should be compared with the horizontal volume flow per unit of height, which is

$$\int_{-d}^{d} u \, \mathrm{d}z = -\frac{2}{3}\frac{d^3}{\mu}\frac{\partial p}{\partial x}. \tag{11}$$

Clearly the function $f(\omega)$ is a measure of the effectiveness of the pressure gradient in producing a vertical flow. The function is presented in table 1. The decrease in effectiveness with increasing stratification (increasing $\omega$) is quite obvious.

The final stage of this part of the calculation is the determination of the pressure in the slot. The pressure distribution is governed by the requirement that mass be conserved in the slot. Let the quantity $Q''(x, y)\,\mathrm{d}A$ be the rate at which fluid is introduced by some external agent into the slot, where $\mathrm{d}A$ is the element of surface across which the fluid crosses. This may be an inlet or exit from a ventilation system or vent, or a cutout in an end wall. Using (10) and (11), the conservation of mass yields the following equation for the pressure:

$$\frac{\partial^2 p}{\partial x^2} + f(\omega)\frac{\partial^2 p}{\partial y^2} = -\frac{3}{2}\frac{\mu}{d^3}Q''(x, y). \tag{12}$$

There are three situations covered by (12) which are of interest. First, if there is no opening into or out of the slot, then $Q'' = 0$. Secondly, if the flux through the opening is specified, then $Q''$ is a prescribed function. One such case of practical interest is a small opening at $x = x_0$, $y = y_0$ for which a total flow rate $Q_0$ is specified, the dimensions being small compared with the length or height of the slot. Then $Q''$ is given by

$$Q''(x, y) = Q_0\,\delta(x - x_0)\,\delta(y - y_0). \tag{13}$$

Here $\delta$ denotes the Dirac delta function. Finally, if the opening is large and the pressure is specified at the opening, then it is more convenient to consider the boundary of the opening as a boundary of the slot along which the pressure is specified. Then $Q'' = 0$ as before over the interior of the region of interest. However, the solution now must be obtained over the rectangular slot, with the correct pressure being specified at the open edge. The second and third cases are complementary in that the flow is specified and the pressure is calculated in the second instance; while the pressure is specified and the flow is calculated in the third.

## 4. The slot pressure distribution

The starting point for the analysis is (12), with $Q'' = 0$. The boundary condition at the closed end of each slot is (see (11) and figure 4)

$$\frac{\partial p}{\partial x}(\tfrac{1}{2}l, y) = 0. \tag{14}$$

At the open end the pressure must be compatible with the end void pressure at that height. If the end-void pressure at the $n$th slot is denoted by $p_v(n, y)$; then the boundary condition at the open end is

$$p(-\tfrac{1}{2}l, y) = p_v(n, y). \tag{15}$$

At the bottom, since there is no flow through the floor of the hold, the boundary condition is (see (10))

$$\frac{\partial p}{\partial y}(x, 0) = 0. \tag{16}$$

Rather than consider the geometry of the air gap at the top of the hold and its interaction with the upper boundary of the slot, it is more convenient to note that most cases of practical interest correspond to value of $\omega$ (see (6)) such that $f(\omega) \ll 1$. If $l/h$ is of order unity, then (12) and (14) imply that, away from the top or bottom of the slot, $p$ depends only on $y$. Let $Q_n$ be the total flow of air drawn through the $n$th slot. Then (10) and (12) imply that the pressure distribution over most of each slot is given by

$$p = \frac{3}{2}\frac{\mu Q_n y}{d_n^3 l_n f(\omega_n)}. \tag{17}$$

Now the same relation must hold in most of the end void, away from the top or bottom. This means that the total flow $Q$ drawn through the hold by the ventilation system can be related to $p$ by the formulae

$$Q \equiv \sum_{n=0}^{N} Q_n = \frac{2}{3}\frac{\rho}{\mu y}\sum_{n=0}^{N} d_n^3 l_n f(\omega_n). \tag{18}$$

The sum in (18) is assumed to extend over all slots and the end void. Eliminating the pressure from this expression yields the result

$$Q_n = \frac{Q l_n d_n^3 f(\omega_n)}{\sum_{n=0}^{N} d_n^3 l_n f(\omega_n)}. \tag{19}$$

Equation (19) is extremely important in what follows. It permits the flow in each slot to be related to the total flow $Q$ drawn through the hold. Thus, since $Q$ is a prescribed system parameter, $Q_n$ can be determined in advance as a function of the hold geometry and stratification. Physically, (17)–(19) mean that the stratification completely suppresses horizontal motion everywhere except near the top and bottom of each slot and the end void. Equation (12) then implies that the horizontal motion is only important in layers of order $l_n[f(\omega_n)]^{\frac{1}{2}}$ in height near the top and bottom. The details of the motion near the top are of no interest. The only thing that matters is that the ventilation air enters there. The bottom horizontal motion must be calculated because it determines the pickup of evaporated spill material. However, it can now be calculated as if the slot were semi-infinite in height with the boundary condition as $y \to \infty$ given by (17).

To carry out the calculation it is appropriate to proceed more formally. Let the pressure in the $n$th slot be made non-dimensional as follows:

$$p = \frac{3}{2}\frac{\mu}{d_n^3}\frac{Q_n}{[f(\omega_n)]^{\frac{1}{2}}}\tilde{p}(\tilde{x},\tilde{y}), \quad \tilde{x} = \frac{x}{l_n}, \quad \tilde{y} = \frac{y}{l_n[f(\omega_n)]^{\frac{1}{2}}}. \tag{20a,b,c}$$

Then the boundary-value problem can be stated in the form

$$\frac{\partial^2\tilde{p}}{\partial\tilde{x}^2}+\frac{\partial^2\tilde{p}}{\partial\tilde{y}^2} = 0, \quad \frac{\partial\tilde{p}}{\partial\tilde{x}}(\tfrac{1}{2},\tilde{y}) = 0, \quad \frac{\partial\tilde{p}}{\partial\tilde{y}}(\tilde{x},0) = 0, \tag{21a,b,c}$$

$$\lim_{\tilde{y}\to\infty}\tilde{p}(\tilde{x},\tilde{y}) = \tilde{y}, \quad \tilde{p}(-\tfrac{1}{2},\tilde{y}) = \tilde{p}_{\mathrm{v}}(n,\tilde{y}), \tag{21d,e}$$

Since the dimensionless end-void pressure $\tilde{p}_{\mathrm{v}}(n,\tilde{y})$ is unknown at this point, it is desirable to seek the solution in a form that displays the dependence on $\tilde{p}_{\mathrm{v}}(n,\tilde{y})$ explicitly. This can be done with the aid of a Green function $G(\tilde{x},x_0,\tilde{y},y_0)$ defined as the solution of the problem

$$\frac{\partial^2 G}{\partial\tilde{x}^2}+\frac{\partial^2 G}{\partial\tilde{y}^2} = \delta(\tilde{x}-x_0)\,\delta(\tilde{y}-y_0), \tag{22a}$$

$$\frac{\partial G}{\partial\tilde{x}}(\tfrac{1}{2},\tilde{y}) = \frac{\partial G}{\partial\tilde{y}}(\tilde{x},0) = 0, \tag{22b}$$

$$G(-\tfrac{1}{2},\tilde{y}) = \lim_{\tilde{y}\to\infty} G(\tilde{x},\tilde{y}) = 0. \tag{22c}$$

Introduce $p$ and $G$ as defined by (21) and (22) into the divergence theorem in the form

$$\oint(\tilde{p}\,\Delta G - G\,\Delta\tilde{p})\,\mathrm{d}x_0\,\mathrm{d}y_0 = \oint\left(\tilde{p}\frac{\partial G}{\partial n_0}-G\frac{\partial\tilde{p}}{\partial n_0}\right)\mathrm{d}S_0. \tag{23}$$

Here $n_0$ denotes the outward pointing normal to the closed contour composed of the slot boundaries and a fixed large value of $y_0$. Now letting $y_0\to\infty$ and using (21) and (22), a formal solution is obtained for the slot pressure $\tilde{p}(\tilde{x},\tilde{y})$ as

$$\tilde{p}(\tilde{x},\tilde{y}) = -\int_0^\infty \tilde{p}_{\mathrm{v}}(n,y)\frac{\partial G}{\partial x_0}(-\tfrac{1}{2},y_0;\tilde{x},\tilde{y})\,\mathrm{d}y_0. \tag{24}$$

In order to make (24) useful, it is necessary to determine $G$ and $\tilde{p}_{\mathrm{v}}$. The solution for $G$ is independent of $\tilde{p}_{\mathrm{v}}$, and only involves the slot geometry. The solution for $\tilde{p}_{\mathrm{v}}$ will be obtained in §5. The Green function $G(\tilde{x},\tilde{y},x_0,y_0)$ can now be obtained with the aid of a sequence of conformal mappings. The steps in the sequence are (see figure 5 for sketches of the mappings)

(i) $\tau = \sin\pi\zeta, \quad \zeta = \tilde{x}+\mathrm{i}\tilde{y}.$

This transforms the slot into a half-space with the open end of the bottom at $\tau = -1$ (figure 5*b*).

(ii) $\tau_1 = \tau+1.$

This moves the open end of the bottom to the origin (figure 5*c*).

(iii) $W = \xi+\mathrm{i}\eta = \tau_1^{\frac{1}{2}}.$

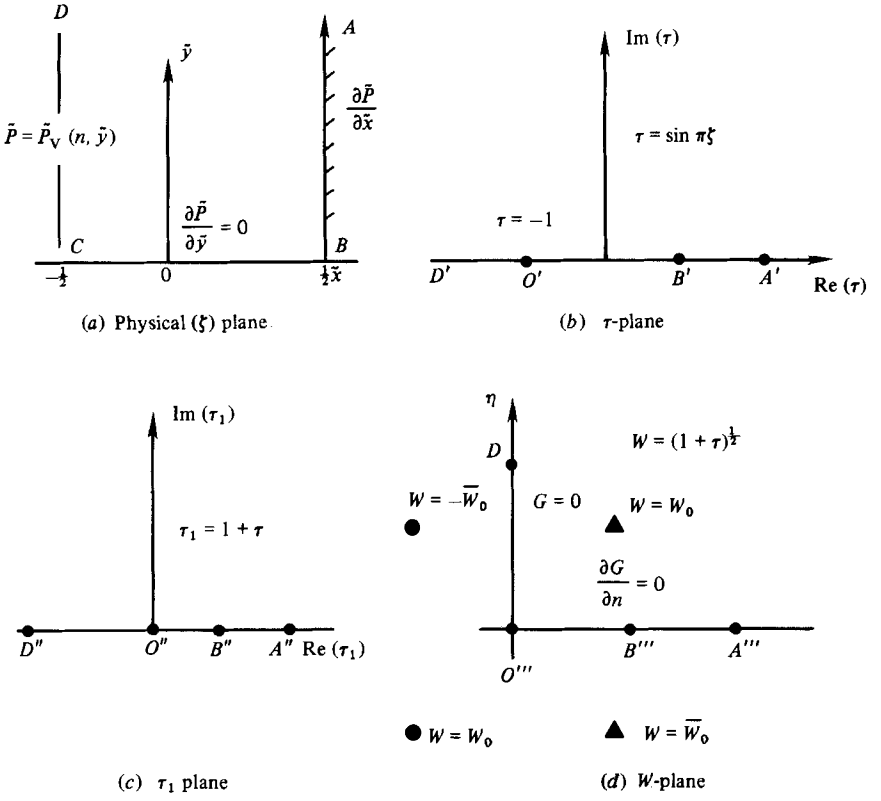


FIGURE 5. Conformal mappings used to obtain the Green function $G$ in (24).

This converts the slot into a quarter-plane with the open end on the positive imaginary axis (figure 5*d*). Thus

$$W = \xi + i\eta = 1 + \sin(\pi\zeta)^{\frac{1}{2}}, \quad \xi = \{\tfrac{1}{2}[a + (a^2 + b^2)^{\frac{1}{2}}]\}^{\frac{1}{2}}, \quad \eta = \{\tfrac{1}{2}[(a^2 + b^2)^{\frac{1}{2}} - a]\}^{\frac{1}{2}}, \tag{25a,b,c}$$

$$a = 1 + \sin \pi\tilde{x} \cosh \pi\tilde{y}, \quad b = \cos \pi\tilde{x} \sinh \pi\tilde{y}. \tag{25d,e}$$

The Green function can be written down immediately in the $W$-plane. A solution is required with a logarithmic singularity at a point $\tilde{x} = x_0$, $\tilde{y} = y_0$ which vanishes for $\xi = 0$ and whose normal derivative vanishes for $\eta = 0$. The solution must be odd in $\xi$ and even in $\eta$. The result is readily obtained in complex form as

$$G + iJ = \frac{1}{2\pi}\{\log(W - W_0) + \log(W - \overline{W}_0) - \log(W + \overline{W}_0) - \log(W + W_0)\}, \tag{26a}$$

$$W_0 \equiv W(x_0, y_0) = \xi(x_0, y_0) + i\eta(x_0, y_0), \tag{26b}$$

$$\overline{W}_0 \equiv \xi(x_0, y_0) - i\eta(x_0, y_0). \tag{26c}$$

Equations (24) and (26) constitute the solution for the pressure in the slot once the end void pressure is known. For later use it is necessary to compute the pressure gradient along the bottom of the slot. This calculation requires considerable care,

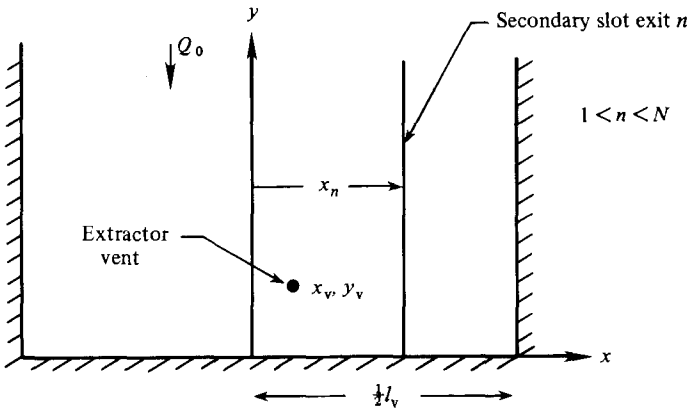


FIGURE 6. Plan view to the end void showing the location of the forced ventilation extraction point (suction). Ventilation flow enters from the top of the void and from the intercontainer slots (one of $N$ slots indicated by a vertical line).

owing to the nearly singular nature of the integral. The result, after considerable algebra, is

$$\frac{\partial \tilde{p}}{\partial \tilde{x}}(x,0) = \frac{\cos \pi\tilde{x}}{(1+\sin \pi\tilde{x})^{\frac{1}{2}}} K(\tilde{x}), \tag{27a}$$

$$K(\tilde{x}) = \int_0^\infty \frac{\mathrm{d}\tilde{p}_v}{\mathrm{d}y_0}(y_0) \frac{(\cosh \pi y_0 - 1)^{\frac{1}{2}} \mathrm{d}y_0}{\sin \pi\tilde{x} + \cosh \pi y_0}. \tag{27b}$$

## 5. The end-void pressure

The final stage in the determination of the large-scale motion is the calculation of the end-void pressure distribution. In order to proceed, it is necessary to assume that the end void can be treated in the same manner as the slots between container stacks, even though in many applications the relevant void width $d_v$ and length $l_v$ are such that the ratios $d_v/l_v$ and $d_v/h$ are not small. If these parameters are assumed to be small, then (12) applies, with $x$ now measuring horizontal distance along the end void. The major difference between the slots and the end void lies in the appearance of non-trivial sources and sinks $Q''(x, y)$ in the end void.

The slots between container stacks are narrow compared with the length or height of the end void. Hence the fluid issuing from them can be represented as line sources of fluid in the form

$$Q''_{\mathrm{slot}}(n) = Q_n \delta(x - x_n) q_n(y). \tag{28}$$

Here $Q_n$ is the total flux issuing from the $n$th slot, as given by (19), and $q_n(y)$ determines the distribution of flow with respect to height. The distribution function $q_n(y)$ is normalized so that

$$\int_0^\infty q_n(y)\,\mathrm{d}y = 1.$$

The air-extraction system is assumed to have physical dimensions that are small compared with the dimensions of the end void. Hence it can be represented as a delta-function sink of strength $Q$, since it exhausts all the air drawn into the hold. The geometry is sketched in figure 6.

The pressure in the end void is then determined by the solution to the following system of equations:

$$\frac{\partial^2 p}{\partial x^2}+f(\omega_v)\frac{\partial^2 p}{\partial y^2}=-\frac{3}{2}\frac{\mu}{d_v^3}Q''(x,y), \tag{29a}$$

$$Q''(x,y)=\sum_{n=1}^{N} Q_n\,\delta(x-x_n)\,q_n(y)-Q\delta(x-x_v)\,\delta(y-y_v), \tag{29b}$$

$$\frac{\partial p}{\partial x}\left(\frac{l_v}{2},y\right)=\frac{\partial p}{\partial x}\left(-\frac{l_v}{2},y\right)=0,\quad \frac{\partial p}{\partial y}(x,0)=0, \tag{29c,d}$$

$$\lim_{y\to\infty} p(x,y)=\frac{3}{2}\frac{\mu Q_0 y}{d_v^3 l_v f(\omega_v)}. \tag{29e}$$

Here $(x_v, y_v)$ is the location of the air extractor, and $Q_0$ is the flow which originates in the end void, as determined by (19) with the void geometric parameters.

The solution procedure is similar to that employed in §4. The equations are made non-dimensional in the form

$$p=\frac{3}{2}\frac{\mu}{d_v^3}\frac{Q_0}{[f(\omega_v)]^{\frac{1}{2}}}\tilde{p}(\tilde{x},\tilde{y}),\quad \tilde{x}=\frac{x}{l_v},\quad \tilde{y}=\frac{y}{l_v[f(\omega_v)]^{\frac{1}{2}}} \tag{30a,b,c}$$

$$\frac{\partial^2\tilde{p}}{\partial\tilde{x}^2}+\frac{\partial^2\tilde{p}}{\partial\tilde{y}^2}=-\sum_{n=1}^{N}\frac{Q_n}{Q_0}\delta(\tilde{x}-\tilde{x}_n)\,q_n(\tilde{y})+\left(1+\sum_{n=1}^{N}\frac{Q_n}{Q_0}\right)\delta(\tilde{x}-\tilde{x}_v)\,\delta(\tilde{y}-\tilde{y}_v), \tag{30d}$$

$$\frac{\partial p}{\partial\tilde{x}}(\pm\tfrac{1}{2},\tilde{y})=\frac{\partial p}{\partial\tilde{y}}(\tilde{x},0)=0,\quad \lim_{\tilde{y}\to\infty}\tilde{p}(\tilde{x},\tilde{y})=\tilde{y}. \tag{30e,f}$$

A Greens function is again introduced, this time solving the following system of equations:

$$\frac{\partial^2 G}{\partial\tilde{x}^2}+\frac{\partial^2 G}{\partial\tilde{y}^2}=\delta(\tilde{x}-\tilde{x}_0)\,\delta(\tilde{y}-\tilde{y}_0),\quad \frac{\partial G}{\partial\tilde{x}}(\tilde{x}=\pm\tfrac{1}{2},\tilde{y},\tilde{x}_0,\tilde{y}_0)=0, \tag{31a,b}$$

$$\frac{\partial G}{\partial\tilde{y}}(\tilde{x},0,\tilde{x}_0,\tilde{y}_0)=0,\quad \lim_{\tilde{y}\to\infty}G(\tilde{x},\tilde{y},\tilde{x}_0,\tilde{y}_0)=y. \tag{31c,d}$$

Substitution of (30) and (31) into (23) then yields the result

$$\tilde{p}(\tilde{x},\tilde{y})=\left(1+\sum_{n=1}^{N}\frac{Q_n}{Q_0}\right)G(\tilde{x},\tilde{y},\tilde{x}_v,\tilde{y}_v)-\sum_{n=1}^{N}\frac{Q_n}{Q_0}\int_0^\infty q_n(\tilde{y}_0)\,G(\tilde{x},\tilde{y},\tilde{x}_n,\tilde{y}_0)\,\mathrm{d}\tilde{y}_0. \tag{32}$$

The solution is completed by specifying $G$ and $q_n$. The Greens function is determined by noting that the first of the transformations employed in the previous section maps the end void into a half-plane. The solution for $G$ is then readily obtained as

$$G+\mathrm{i}J=\frac{1}{2\pi}\{\log(\tau-\tau_0)+\log(\tau-\bar{\tau}_0)\}, \tag{33a}$$

$$\tau=\sin\pi\zeta=\sin\pi\tilde{x}\cosh\pi\tilde{y}+\mathrm{i}\cos\pi\tilde{x}\sinh\pi\tilde{y}, \tag{33b}$$

$$\tau_0=\sin\pi\tilde{x}_0\cosh\pi\tilde{y}_0+\mathrm{i}\cos\pi\tilde{x}_0\sinh\pi\tilde{y}_0, \tag{33c}$$

$$\bar{\tau}_0=\sin\pi\tilde{x}_0\cosh\pi\tilde{y}_0-\mathrm{i}\cos\pi\tilde{x}_0\sinh\pi\tilde{y}_0. \tag{33d}$$

The flow-distribution functions $q_n$ are in reality not arbitrary, but must be determined by the condition that the pressure as computed from (32) and (33) lead to the same flows when the solutions given by these equations are substituted into

(24) and (24) is differentiated to obtain the flow out of each slot. In general this leads to a system of $N$ integral equations for the void pressure at each slot. The solution can be approximated with reasonable accuracy (i.e. enough accuracy to evaluate (27)) by noting several points. First, the fact that the total flow issuing from each slot is known implies the constraint given above on $q_n(y)$. Secondly, the flow should be greatest at height $\tilde{y} = \tilde{y}_v$, since that is the level at which the air is drawn out. Thirdly, the flow should ultimately decay exponentially with distance away from its maximum, since the integral equations have the Green functions for kernels, and the Green functions all exhibit this type of decay. Finally, examination of (27) and (32) shows that the pressure cannot be sensitive to details of the shape of $q_n(\tilde{y})$. Hence, in the spirit of Carrier (1965), the following form for $q_n(\tilde{y})$ is postulated:

$$q_n(\tilde{y}) = \frac{\pi}{2 - e^{-\pi \tilde{y}_v}} \exp\{-\pi |\tilde{y} - \tilde{y}_v|\}. \tag{34}$$

Equation (34) is consistent with all the points mentioned above. It also permits the integral in (32) to be evaluated in closed form. The result, after some extremely tedious algebra, is

$$\tilde{p}(\tilde{x}, \tilde{y}) = \left(1 + \sum_{n=1}^{N} \frac{Q_n}{Q_0}\right) G(\tilde{x}, \tilde{y}; \tilde{x}_v, \tilde{y}_v) + \sum_{n=1}^{N} \frac{Q_n}{Q_0} \frac{1}{2\pi(2 - e^{-\pi \tilde{y}_v})} \left\{ \sum_{j=1}^{4} L(t_j) - \tfrac{1}{2}(2 - e^{-\pi \tilde{y}_v}) \log[(1 - a_j)^2 + b_j^2] \right\}, \tag{35a}$$

$$L(t_j) = 1 + e^{\pi \tilde{y}_v} \left\{ \frac{a_j}{2} \log\left[\frac{(e^{-\pi \tilde{y}_v} - a_j)^2 + b_j^2}{a_j^2 + b_j^2}\right] + |b_j| \left[\arctan \frac{a_j - e^{-\pi \tilde{y}_v}}{|b_j|} - \arctan \frac{a_j}{|b_j|}\right] \right\}$$
$$+ \log\left[\frac{(1 - a_j)^2 + b_j^2}{(e^{-\pi \tilde{y}_v} - a_j)^2 + b_j^2}\right] - \tfrac{1}{2} a_j \frac{e^{-\pi \tilde{y}_v}}{a_j^2 + b_j^2} \log \frac{(1 - a_j)^2 + b_j^2}{(1 - a_j e^{\pi \tilde{y}_v})^2 + (b_j e^{\pi \tilde{y}_v})^2}$$
$$- \frac{e^{-\pi \tilde{y}_v} |b_j|}{a_j^2 + b_j^2} \arctan \frac{a_j - e^{-\pi \tilde{y}_v}}{|b_j|} - \arctan \frac{a_j - 1}{|b_j|} \Bigg\}, \tag{35b}$$

$$a_1 = -e^{\pi \tilde{y}} \cos \pi(\tilde{x} + \tilde{x}_n), \quad b_1 = e^{\pi \tilde{y}} \sin \pi(\tilde{x} + x_n), \tag{35c,d}$$

$$a_2 = e^{-\pi \tilde{y}} \cos \pi(\tilde{x} - \tilde{x}_n), \quad b_2 = e^{-\pi \tilde{y}} \sin \pi(\tilde{x} - \tilde{x}_n), \tag{35e,f}$$

$$a_3 = -e^{-\pi \tilde{y}} \cos \pi(\tilde{x} + \tilde{x}_n), \quad b_3 = e^{-\pi \tilde{y}} \sin \pi(\tilde{x} + \tilde{x}_n), \tag{35g,h}$$

$$a_4 = e^{\pi \tilde{y}} \cos \pi(\tilde{x} - \tilde{x}_n), \quad b_4 = e^{\pi \tilde{y}} \sin \pi(\tilde{x} - \tilde{x}_n). \tag{35i,j}$$

## 6. The bottom motion

When the vertical distance above the hold bottom becomes comparable to the slot width, the flow pattern departs from that calculated in previous sections. While the length $l$ of the slot is still long compared with the half-width $d$, the vertical scale is now of order $d$ since the downward flow must terminate at the bottom. The boundary layers at the sides of each slot, which carry the ventilation air downward, must spill out into the bottom across the full width of the slot. The horizontal motion must also adjust so that it can come to rest at the bottom.

To proceed, we consider the *dimensional* dependent variables introduced in (2).

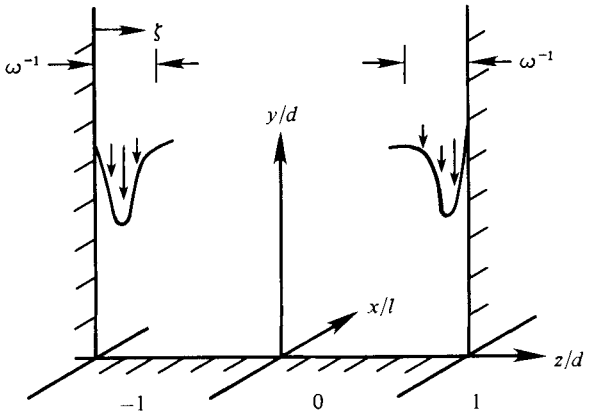


FIGURE 7. Cross-section of the bottom of an intercontainer slot. The velocity distribution of the gas as it approaches the slot bottom is indicated next to each wall.

Substituting these into the linearized form of (1) (recall that $Re = O(1)$), the equations of motion become

$$\frac{\partial u}{\partial x}+\frac{\partial v}{\partial y}+\frac{\partial w}{\partial z}=0, \quad \frac{\partial p}{\partial x}=\mu\,\Delta u, \tag{36a,b}$$

$$\frac{\partial p}{\partial y}-\frac{\rho g}{T_0}\theta=\mu\,\Delta v, \quad \frac{\partial p}{\partial z}=\mu\,\Delta w, \quad \frac{T_1-T_0}{h}v=\frac{\mu}{\rho\,Pr}\Delta\theta. \tag{36c,d,e}$$

The geometry is shown schematically in figure 7. Equations (36) are to be solved subject to the following boundary conditions:

$$u(x,y,\pm d)=u(x,0,z)=0, \quad v(x,y,\pm d)=v(x,0,z)=0, \tag{37a,b}$$

$$w(x,y,\pm d)=w(x,0,z)=0, \quad \theta(x,y,\pm d)=\theta(x,0,z)=0. \tag{37c,d}$$

Finally, for $y \gg d$ the solutions for $u$, $v$, $w$ and $\theta$ must merge smoothly with those obtained in §§2–5. This statement will be made in a more quantitative fashion below.

The solution procedure is based on explicitly recognizing the differences between the four relevant lengthscales in the problem. These scales are, in decreasing order of magnitude:

(1) the slot length $l$;
(2) the scale height $l[f(\omega)]^{\frac{1}{2}}$ for large-scale motion;
(3) the slot half-width $d$;
(4) the slot-wall boundary-layer thickness $d/\omega$.

The slot bottom region is now divided into two wall boundary layers and an interior region. In the interior region the dependent variables are expanded in an ascending series in the parameter $d/l$ of the form:

$$p=\frac{3}{2}\frac{\mu Q_0}{d^3[f(\omega)]^{\frac{1}{2}}}\{\tilde{p}(\tilde{x},0)+\left(\frac{d}{l}\right)^2 p^*(\tilde{x},Y,Z)+\ldots\}, \tag{38a}$$

$$u=\frac{3}{2}\frac{Q_0}{ld[f(\omega)]^{\frac{1}{2}}}\{u^*(\tilde{x},Y,Z)+\ldots\}, \tag{38b}$$

$$v=\frac{3}{2}\frac{Q_0}{ld[f(\omega)]^{\frac{1}{2}}}\frac{d}{l}\{v^*(\tilde{x},Y,Z)+\ldots\}, \tag{38c}$$

$$w = \frac{3}{2}\frac{Q_0}{ld[f(\omega)]^{\frac{1}{2}}}\frac{d}{l}\{w^*(\tilde{x}, Y, Z)+\ldots\}, \tag{38d}$$

$$\theta = \frac{T_0}{\rho g d}\frac{3}{2}\frac{\mu Q_0}{d^3[f(\omega)]^{\frac{1}{2}}}\left(\frac{d}{l}\right)^2\{\theta^*(\tilde{x}, Y, Z)+\ldots\}, \tag{38e}$$

$$\tilde{x} = \frac{x}{l}, \quad Y = \frac{y}{d}, \quad Z = \frac{z}{d}. \tag{38f,g,h}$$

Note that in (38) $\tilde{p}(\tilde{x}, 0)$ is the pressure obtained from the calculation of the large-scale motion in §4. The velocity components and temperature are scaled to ensure consistency with the large-scale motion and with each other. Substitution of (38) into (36) and ignoring terms of order $(d/l)^2$ yields

$$\frac{\partial u^*}{\partial \tilde{x}}+\frac{\partial v^*}{\partial Y}+\frac{\partial w^*}{\partial Z} = 0, \quad \frac{\partial \tilde{p}}{\partial \tilde{x}}(\tilde{x}, 0) = \frac{\partial^2 u^*}{\partial Y^2}+\frac{\partial^2 u^*}{\partial Z^2}, \quad \frac{\partial p^*}{\partial Y}-\theta^* = \frac{\partial^2 u^*}{\partial Y^2}+\frac{\partial^2 w^*}{\partial Z^2} \tag{39a,b,c}$$

Since the driving force in (39), $\partial\tilde{p}(\tilde{x}, 0)/\partial\tilde{x}$ is known, the velocity component $u^*$ in the direction of the slot can be obtained seprately from the other variables, as the solution of

$$\frac{\partial^2 u^*}{\partial Y^2}+\frac{\partial^2 u^*}{\partial Z^2} = \frac{\partial \tilde{p}}{\partial \tilde{x}}(\tilde{x}, 0), \tag{40a}$$

$$u^*(\tilde{x}, 0, Z) = u^*(\tilde{x}, Y, -1) = u^*(\tilde{x}, Y, +1) = 0, \tag{40b}$$

$$\lim_{y\to\infty} u^*(\tilde{x}, Y, Z) = -\frac{1}{2}\frac{\partial \tilde{p}}{\partial x}(\tilde{x}, 0)(1-Z^2) \tag{40c}$$

(recall (8*b*)). To proceed, $u^*$ is written as the sum of the large-scale motion near the bottom plus a correction:

$$u^* = -\frac{1}{2}\frac{\partial \tilde{p}}{\partial \tilde{x}}(\tilde{x}, 0)(1-Z^2)+\bar{u}, \quad \frac{\partial \bar{u}^2}{\partial Y^2}+\frac{\partial \bar{u}^2}{\partial Z^2} = 0, \tag{41a,b}$$

$$\bar{u}(\tilde{x}, Y, -1) = \bar{u}(\tilde{x}, Y, +1) = 0, \tag{41c}$$

$$\bar{u}(\tilde{x}, 0, Z) = \frac{1}{2}\frac{\partial \tilde{p}}{\partial \tilde{x}}(\tilde{x}, 0)(1-Z^2), \quad \lim_{Y\to\infty} \bar{u} = 0. \tag{41d,e}$$

The correction $\bar{u}$ can be expressed in terms of a Green function $G(Y, Z; Y_0, Z_0)$ in a manner analogous to that described in previous sections. The result of the calculation is

$$\bar{u}(\tilde{x}, Y, Z) = -\frac{1}{2}\frac{\partial \tilde{p}}{\partial \tilde{x}}(\tilde{x}, 0)\int_{-1}^{1} dZ_0\,(1-Z_0^2)\frac{\partial G}{\partial Y_0}(Y, Z; 0, Z_0), \tag{42a}$$

$$G+iJ = \frac{1}{2\pi}\{\log(\phi-\phi_0)-\log(\phi-\bar{\phi}_0)\}, \tag{42b}$$

$$\phi = \sin\pi\lambda, \quad \lambda = Z+iY, \tag{42c,d}$$

$$\phi_0 = \sin\pi\lambda_0, \quad \lambda_0 = Z_0+iY_0, \tag{42e,f}$$

$$\bar{\phi}_0 = \sin\pi\bar{\lambda}_0, \quad \bar{\lambda}_0 = Z_0-iY_0. \tag{42g,h}$$

The final expression for $u^*$ can be rewritten in a more convenient form for

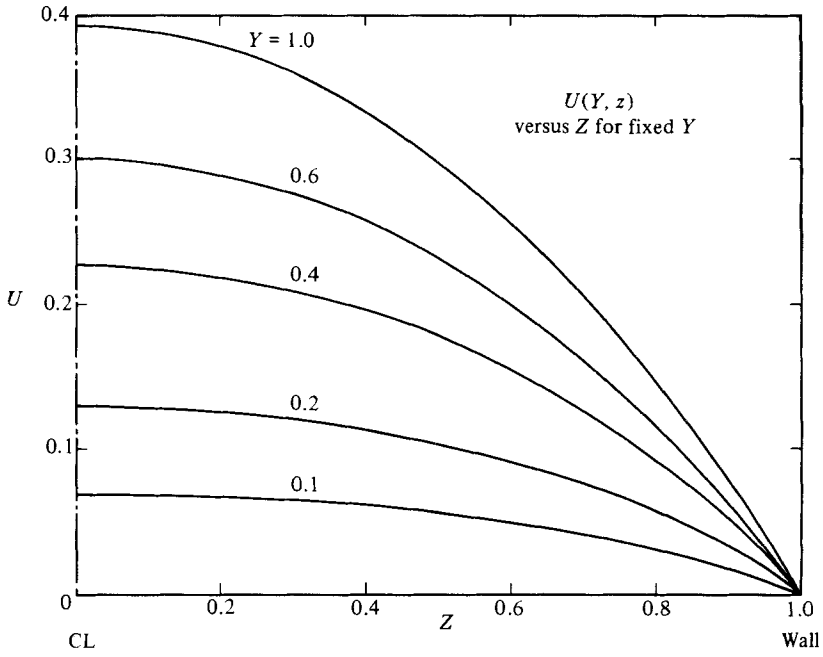


FIGURE 8. Universal velocity profiles for the axial flow in the boundary layer of a slot bottom. The flow is symmetrical about the slot centreline, so only one-half the slot width is shown. The velocity is zero at the slot bottom and increases toward an asymptotic profile as height $y$ above the bottom increases.

computation by employing the Cauchy–Riemann equations to eliminate $\partial G/\partial Y_0$. The result is

$$u^*(\tilde{x}, Y, Z) = -\frac{\partial \tilde{p}}{\partial \tilde{x}}(\tilde{x}, 0)\{\tfrac{1}{2}(1-Z^2) - \int_{-1}^{1} \mathrm{d}Z_0\, Z_0\, J(Y, Z; 0, Z_0)\}, \tag{43a}$$

with

$$J = \frac{1}{\pi}\arctan\frac{I(Z, Y)}{R(Z, Y) - R(Z_0, 0)} \quad \text{if} \quad R(Z, Y) > R(Z_0, 0), \tag{43b}$$

and

$$J = \frac{1}{\pi}\left\{\pi - \arctan\frac{I(Z, Y)}{R(Z_0, 0) - R(Z, Y)}\right\} \quad \text{if} \quad R(Z_0, 0) > R(Z, Y). \tag{43c}$$

The quantities $I$ and $R$ are given by

$$R(Z, Y) = \sin\tfrac{1}{2}\pi Z \cosh\tfrac{1}{2}\pi Y, \quad I(Z, Y) = \cos\tfrac{1}{2}\pi Z \sinh\tfrac{1}{2}\pi Y. \tag{44a,b}$$

Note that $u^*$ as given by (43) and (44) has the form

$$u^* = -\frac{\partial \tilde{p}}{\partial \tilde{x}}(\tilde{x}, 0)\, U(Y, Z). \tag{45}$$

Thus the velocity profile at each axial station $\tilde{x}$ = constant has the same 'universal profile' $U(Y, Z)$. This profile is displayed in figure 8. The $\tilde{x}$-dependence can be factored out of all the variables in (39); the resulting decomposition being given by

$$v^* = \frac{\partial^2 \tilde{p}}{\partial \tilde{x}^2}(\tilde{x}, 0)\, V(Y, Z), \quad w^* = \frac{\partial^2 \tilde{p}}{\partial \tilde{x}^2}(\tilde{x}, 0)\, W(Y, Z), \tag{46a,b}$$

$$\theta^* = \frac{\partial^2 \tilde{p}}{\partial \tilde{x}^2}(\tilde{x}, 0)\, \theta(Y, Z), \quad p^* = \frac{\partial^2 \tilde{p}}{\partial \tilde{x}^2}(\tilde{x}, 0)\, P(Y, Z). \tag{46c,d}$$

The profile functions $V$, $W$, $\theta$ and $P$ satisfy

$$\frac{\partial V}{\partial Y}+\frac{\partial W}{\partial Z}=U, \quad \frac{\partial P}{\partial Z}=\frac{\partial^2 W}{\partial Y^2}+\frac{\partial^2 W}{\partial Z^2}, \tag{47a,b}$$

$$\frac{\partial P}{\partial Y}-\theta=\frac{\partial^2 V}{\partial Y^2}+\frac{\partial^2 V}{\partial Z^2}, \quad \omega^4 V=\frac{\partial^2 \theta}{\partial Y^2}+\frac{\partial^2 \theta}{\partial Z^2}. \tag{47c,d}$$

In order to proceed further, it is necessary to consider the dependence of the solutions on $\omega$. In particular, the structure of the wall boundary layers (of thickness $\omega^{-1}$ on the slot half-width scale) must be determined (see figure 7). The boundary-layer structure can be found from (47) without loss of generality; since the $\tilde{x}$-dependence factors out in the form given by (47) everywhere in the slot bottom. Symmetry considerations then permit attention to be confined to the wall layer near $Z=-1$, the layer near $Z=+1$ being identical. In this region

$$V=\omega\hat{V}(\zeta, Y), \quad W=\hat{W}(\zeta, Y), \tag{48a,b}$$

$$\theta=\omega^3\hat{\theta}(\zeta, Y), \quad P=\omega^3\hat{P}(\zeta, Y), \quad \zeta=\omega(Z+1).$$

Substitution of (48) into (47) and keeping the leading-order terms in $\omega$ leads to the wall boundary-layer equations in the form

$$\frac{\partial \hat{V}}{\partial Y}+\frac{\partial \hat{W}}{\partial \zeta}=0, \quad \frac{\partial \hat{P}}{\partial \zeta}=0, \quad \frac{\partial \hat{P}}{\partial Y}-\hat{\theta}=\frac{\partial^2 \hat{V}}{\partial \zeta^2}, \quad \hat{V}=\frac{\partial^2 \hat{\theta}}{\partial \zeta^2}. \tag{49a,b,c,d}$$

At the wall, $\zeta=0$, the velocity components and the temperature perturbation must vanish (the latter owing to the assumed equilibrium between container stacks and hold stratification). As $\zeta\to\infty$ these solutions must match the expressions for $V$, $W$, $\theta$ and $P$ (which have not yet been found) in the interior of the slot bottom region. For the present we assume only that all quantities are bounded in the interior, as $\zeta\to\infty$.

Equation (49) may be readily solved by noting that, from the second of these equations,

$$\hat{P}=\hat{P}(Y). \tag{50}$$

Although $\hat{P}(Y)$ is as yet unknown, $\hat{V}$ and $\hat{\theta}$ may then be found in terms of $\hat{P}(Y)$ as

$$\hat{\theta}=\frac{\partial P}{\partial Y}\left\{1-\exp\left(-\frac{\zeta}{\sqrt{2}}\right)\cos\frac{\zeta}{\sqrt{2}}\right\}, \quad \hat{V}=-\frac{\partial P}{\partial Y}\exp\left(-\frac{\zeta}{\sqrt{2}}\right)\cos\frac{\zeta}{\sqrt{2}}. \tag{51a,b}$$

Note that as $\zeta\to\infty$ (i.e. as the interior of the bottom region $\theta$ is approached)

$$\hat{\theta}\to\frac{\mathrm{d}\hat{P}}{\mathrm{d}Y}, \quad \hat{W}\to\frac{1}{\sqrt{2}}\frac{\mathrm{d}^2\hat{P}}{\mathrm{d}Y^2}, \quad \hat{V}\to 0. \tag{52a,b,c}$$

In order for the interior functions (the solutions to (47)) to have proper scaling with respect to $\omega$, they must be consistent with (52) as $Z\to\pm 1$. This can be achieved by rescaling as follows:

$$V(Y,Z)=\omega^{-1}V_{\mathrm{I}}(Y,Z), \quad \theta(Y,Z)=\omega^3\theta_{\mathrm{I}}(Y,Z), \quad P(Y,Z)=\omega^2 P_{\mathrm{I}}(Y,Z) \tag{53a,b,c}$$

The leading terms in the interior equations then become

$$\frac{\partial W}{\partial Z}=U, \quad \frac{\partial P_{\mathrm{I}}}{\partial Z}=0, \quad \frac{\partial P_{\mathrm{I}}}{\partial Y}-\theta_{\mathrm{I}}=0. \tag{54a,b,c}$$

From (54*b*) and (50)

$$P_{\mathrm{I}}=\hat{P}(Y). \tag{55}$$

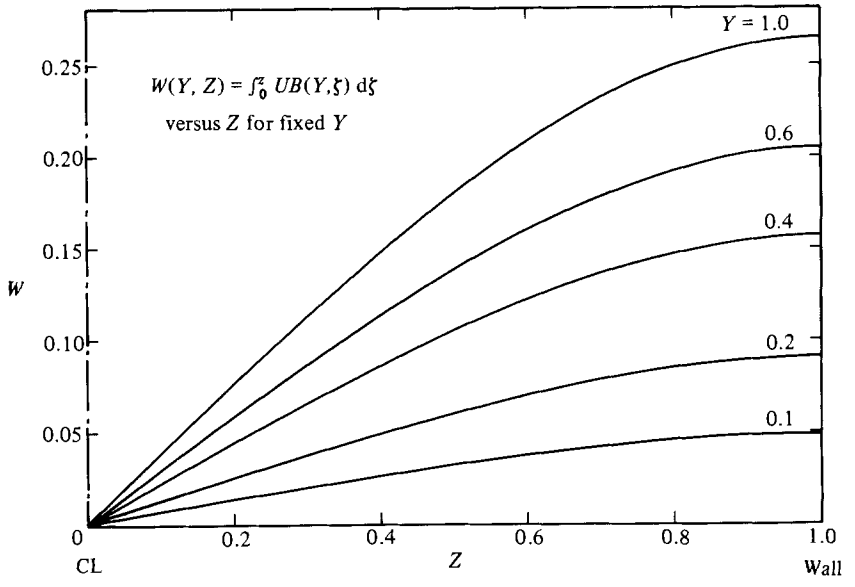


FIGURE 9. Universal velocity profiles for the transverse flow in the boundary layer of a slot bottom. The flow is antisymmetric about the slot centreline, so only one half the slot width is shown. The velocity is zero at the slot bottom and increases toward an asymptotic profile as height $y$ above the slot bottom increases.

Equation (54$c$) is now consistent with (52$a$), yielding the result

$$\theta_I = \frac{\partial \hat{P}}{\partial Y}(Y). \tag{56}$$

Finally, (54$a$) yields

$$W = \int_0^Z U\,dZ,$$

where

$$U = \tfrac{1}{2}(1-Z^2) - \int_{-1}^{1} dZ_0\, Z_0\, J(Y, Z; 0, Z_0) \tag{57}$$

(see (43)).

The transverse profile $W$ is displayed in figure 9. Note that $U$ is symmetric in $Z$, so $W$ is antisymmetric. The remaining unknown $\hat{P}(Y)$ is determined by requiring that $W(\pm 1, Y)$ be consistent with the matching condition given (52$b$). Thus

$$\frac{d^2\hat{P}}{dY^2} = -\sqrt{2}\int_0^1 U(Z, Y)\,dZ. \tag{58}$$

This equation can be integrated once with respect to $Y$, using the value $d\hat{P}(0)/dY = 0$ to ensure that the vertical velocity in the wall layer vanishes at $Y = 0$ (see (51)).

The most important results of this section are (43) and (57), which yield the profiles for the two principal velocity components in the bottom region. These profiles will now be used in the calculation of the vapour pickup in this region.

## 7. The vapour pickup

The calculation of the vapour pickup requires a solution for the vapour concentration gradient at the bottom of the hold. In order to proceed, it is necessary to recall the

spill scenario postulated in §2. It is now further assumed that the bulk of the pickup takes place along the bottom, but outside the wall boundary layers. The concentration $C(x, y, z)$ then obeys the equation

$$u\frac{\partial C}{\partial X}+w\frac{\partial C}{\partial Z}=D\,\Delta C. \tag{59}$$

Here $D$ is the diffusivity of the spill vapour in air and $u$ and $w$ are the velocity components determined in §6. At $y = 0$, the concentration is assumed to be $C_0$, the equilibrium vapour pressure at the temperature corresponding to the hold bottom. Outside the layer there is no vapour: $C = 0$.

We now non-dimensionalize the velocities and coordinates as in (38). The concentration equation (59) then takes the form

$$u^*\frac{\partial C}{\partial \tilde{x}}(\tilde{x},\,Y,Z)+w^*\frac{\partial C}{\partial Z}(\tilde{x},\,Y,Z)=\frac{1}{R_e^*\,S_c}\Delta_2 C, \tag{60a}$$

where

$$\Delta_2 C\equiv\frac{\partial^2 C}{\partial Y^2}+\frac{\partial^2 C}{\partial Z^2},\quad R_e^*=\frac{3Q_0}{2ld[f(\omega)]^{\frac{1}{2}}}\frac{d}{\nu}\frac{d}{l},\quad S_c=\nu/D. \tag{60b,c,d}$$

Equation (60$a$) must be solved subject to the boundary conditions

$$C(\tilde{x},0,Z)=C_0,\quad \lim_{Y\to\infty}C(\tilde{x},\,Y,Z)=0. \tag{61a,b}$$

The solution procedure employed is a generalization to three dimensions of that used by Lighthill (1950) in obtaining his heat-transfer formula. Recall that (45), (46) and (57) allow $u^*$ and $w^*$ to be expressed as

$$u^*=-\frac{\partial\tilde{P}}{\partial\tilde{x}}(\tilde{x},0)\frac{\partial W}{\partial Z}(Y,Z),\quad w^*=\frac{\partial^2\tilde{P}}{\partial\tilde{x}^2}(\tilde{x},0)\,W(Y,Z). \tag{62a,b}$$

Following Lighthill, the vertical dependence of velocity profiles is approximated by a linear function:

$$W(Y,Z)\approx W_0(Z)\,Y,\quad W_0\equiv\left(\frac{\partial W}{\partial Y}\right)_{Y=0}. \tag{63}$$

This approximation may be justified in several ways. First, when the Schmidt number $S_c \gg 1$, it is rigorously true that this simplification yields the asymptotic solution for the concentration profile. Lighthill has shown that, in the case of heat transfer, the approximation works quite well for Prandtl numbers of 0.7, corresponding to air. In the present application $S_c$ is usually in the range $1.5 < S_c < 2$. For this range of Schmidt number the concentration field is largely controlled by the velocity profiles near the bottom. Inspection of figures 8 and 9 shows that the velocity profiles are fairly linear in this region. Finally it should be noted that only the wall concentration gradient is required, not the whole concentration profile. Such information can be (and often is) obtained using much cruder profile information than will emerge from this calculation.

It is convenient to express the velocity components in terms of a stream function $\psi(\tilde{x}, Z)$ defined as

$$\psi(\tilde{x},Z)=-\frac{\partial\tilde{P}}{\partial\tilde{x}}(\tilde{x},0)\,W_0(Z). \tag{64}$$

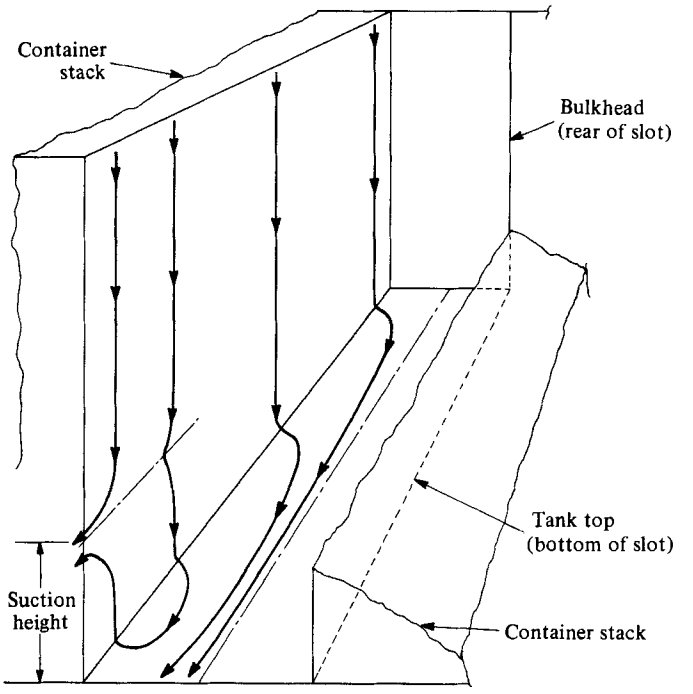


FIGURE 10. Perspective sketch of an intercontainer slot showing air-flow streamlines. The air picks up evaporated spill vapour as it moves in the boundary layer along the bottom of the slot.

The velocity components given by

$$u^* = Y\frac{\partial\psi}{\partial Z}; \quad w^* = -Y\frac{\partial\psi}{\partial\tilde{x}}. \tag{65a,b}$$

The vertical coordinate is now rescaled as follows:

$$\lambda = (R_e^* S_c)^{\frac{1}{3}} Y. \tag{66}$$

The concentration equation now becomes

$$\eta\left\{\frac{\partial\psi}{\partial Z}\frac{\partial C}{\partial\tilde{x}} - \frac{\partial\psi}{\partial\tilde{x}}\frac{\partial C}{\partial Z}\right\} = \frac{\partial^2 C}{\partial\lambda^2}. \tag{67}$$

The solution of (67) depends crucially on the observation that curves of constant $\psi$ represent the trace of the streamlines calculated in §6 on the bottom. These streamlines originate in the wall layer at the side of each container stack. Let $s$ denote distance along each streamline with the origin at the point where the streamline emerges from the wall (see figure 10). Using $s$, $\psi$ as independent variables in place of $\tilde{x}$, $Z$, (67) becomes

$$q(s,\psi)\lambda\frac{\partial C}{\partial s} = \frac{\partial^2 C}{\partial\lambda^2}, \quad q^2 = \left(\frac{\partial\psi}{\partial Z}\right)^2 + \left(\frac{\partial\psi}{\partial\tilde{x}}\right)^2. \tag{68a,b}$$

At $s = 0$ the ventilation air has just entered the bottom region; hence $C = 0$. At $\lambda = 0$ $C = C_0$, and $C \to 0$ as $\lambda \to \infty$ from (61). This is a relatively straightforward problem. To proceed, we introduce a modified streamwise variable $\xi$ defined as

$$\xi = \int_0^s \frac{\mathrm{d}s}{q(s,\psi)}. \tag{69}$$

Then
$$\eta \frac{\partial C}{\partial \xi} = \frac{\partial^2 C}{\partial \lambda^2}. \tag{70}$$

Introducing Laplace transforms with respect to $\xi$, (70) becomes

$$p\lambda \bar{C} = \frac{\partial^2 \bar{C}}{\partial \lambda^2}, \tag{71a}$$

with

$$\bar{C} = \int_0^\infty \mathrm{e}^{-p\xi} C(\xi, \lambda)\, \mathrm{d}\xi, \tag{71b}$$

$$\bar{C}(\xi, 0) = \frac{C_0}{p}, \quad \bar{C} \to 0 \quad \text{as} \quad \eta \to \infty. \tag{71c}$$

The solution for $\bar{C}$ satisfying (71) is readily found (Abramowitz & Stegun 1964) to be

$$\bar{C} = \frac{C_0}{p} \Gamma(\tfrac{2}{3})\, 3^{\frac{2}{3}}\, \mathrm{Ai}\,(p^{\frac{1}{3}}\lambda). \tag{72}$$

Here Ai is the Airy function, and $\Gamma$ the gamma function as defined in Abramowitz & Stegun.

Although inversion of $\bar{C}$ to obtain the concentration profile would be a formidable undertaking, the problem becomes tractable if only the wall concentration gradients are required. The mass flux $\dot{m}$ picked up at each point by the ventilation system is given by

$$\begin{aligned} \dot{m} &= -D \frac{\partial C}{\partial y} \\ &= -\frac{D}{d} (R_{\mathrm{e}}^* S_{\mathrm{c}})^{\frac{1}{3}} \frac{\partial C}{\partial \lambda}. \end{aligned} \tag{73}$$

From (72), the Laplace transform $\overline{\dot{m}}$ is readily computed as:

$$\overline{\dot{m}} = \frac{D}{d} (R_{\mathrm{e}}^* S_{\mathrm{c}})^{\frac{1}{3}} C_0\, 3^{\frac{1}{3}} \frac{\Gamma(\frac{2}{3})}{\Gamma(\frac{1}{3})} p^{-\frac{2}{3}}. \tag{74}$$

Inverting (74) and recalling the definition of $\xi$ from (69), the mass flux becomes

$$\dot{m} = \frac{D}{d} C_0 \frac{3 R_{\mathrm{e}} S_{\mathrm{c}}}{\Gamma(\frac{1}{3})} \left\{ \int_0^S \frac{\mathrm{d}s}{q(s, \psi)} \right\}^{-\frac{1}{3}}, \quad \Gamma(\tfrac{1}{3}) = 2.67894\ldots. \tag{75}$$

Equation (75) yields the pickup at each point in a given slot. The quantity actually desired is the total mass pickup. The total mass pickup in a slot $\dot{M}$ is given by

$$\begin{aligned} \dot{M} &= \int_{-d}^{d} \mathrm{d}z \int_0^l \mathrm{d}x\, \dot{m} \\ &= 2dl \int_0^1 \mathrm{d}Z \int_0^1 \mathrm{d}\tilde{x}\, \dot{m}(\tilde{x}, Z). \end{aligned} \tag{76}$$

Now let $s$ and $n$ be coordinates along and normal to a streamline $\psi$ = constant. Then, from (75) and (76),

$$\dot{M} = dDlC_0 \frac{(3R_{\mathrm{e}}^* S_{\mathrm{c}})^{\frac{1}{3}}}{\Gamma(\frac{1}{3})} \int\int \mathrm{d}s\, \mathrm{d}n \left\{ \int_0^s \frac{\mathrm{d}s}{q(s, \psi)} \right\}^{-\frac{1}{3}}. \tag{77}$$

Using the fact that $dn = d\psi/q$ and $d\xi = ds/q$, it is possible to carry out the integral along streamlines to obtain

$$\dot{M} = \frac{2DlC_0(3R_e^* S_c)^{\frac{1}{3}}}{\Gamma(\frac{1}{3})} \int_0^{\psi_M} d\psi \, \tfrac{3}{2} [\xi(\psi)]^{\frac{2}{3}}, \tag{78a}$$

$$\xi_M(\psi) = \int_0^{s_M(\psi)} \frac{ds}{q}. \tag{78b}$$

Here $s_M(\psi)$ denotes integration over the entire distance along each streamline from the point it enters the bottom until the time it exits into the end void (see figure 10). Similarily, $\psi_M$ denotes the maximum value of the stream function, so that the integration covers all streamlines originating in the wall layer.

At this point it is convenient to recapitulate the overall calculation procedure. The first step is the determination of the flow assigned to each slot and to the end void. This is given by (19), which yields the total flow $Q_n$ in each slot as a function of the total flow drawn through the hold, the hold geometry and the degree of stratification. The next step is the computation of the pressure gradient along the bottom of each slot containing spill material. This pressure gradient controls the development of the spill-material boundary layer, and hence the rate at which spill material is picked up by the ventilation system. The necessary result is given in (27). Note that this formula, in turn, requires a knowledge of the variation of the void pressure $\tilde{p}_v$ with height at the open end of each slot in question. The void pressure at any point is given by (35), which requires only the information already obtained from (19). With the pressure gradient along the slot bottom now determined, the velocity distribution near the slot bottom are given by (43)–(46) and (57). These results are then used to get approximate simplified formulae (63) and (64), which are actually used in the calculation of the rate of pickup of spill material. These latter formulae express the velocities near the bottom of each slot in terms of a 'bottom stream function' $\psi$. Given the quantity $\psi$, the magnitude $q$ of the velocity gradient at each slot bottom can be determined from (68). Finally, given $q$ and $\psi$, (77) yields the total mass pickup in each slot $\dot{M}$. These results, summed over all the slots containing spill material, yield the total mass per unit time extracted from the hold by the ventilation system. The computer program that executes these calculations is of necessity quite elaborate. It is described in Baum & Rockett (1983).

## 8. Numerical results

The purpose of this study was to predict the mass-evaporation rate for a hazardous liquid spill in a containership hold. Since no information was available about the extent of such a spill, it was assumed that the liquid would spread uniformly over the bottom of the hold (tank top). In practice there is almost always some trim to the ship so that liquid would tend to drain to the aft end of the hold. A low-point sump could collect some of the liquid which might be advantageously pumped to a safe place, thus reducing the amount of liquid that would have to be removed by the rather slow evaporation process. Rolling of the ship would tend to spread the spill across the entire width of the hold; the spill was assumed to extend fore and aft along the entire length of the intercontainer slots and athwart ships across all the slots. However, no evaporation was computed for the main void comprising the transverse space between the bulkhead and the end of the container stacks. Unless otherwise noted the calculations were done for a hold containing twelve stacks of 12 m

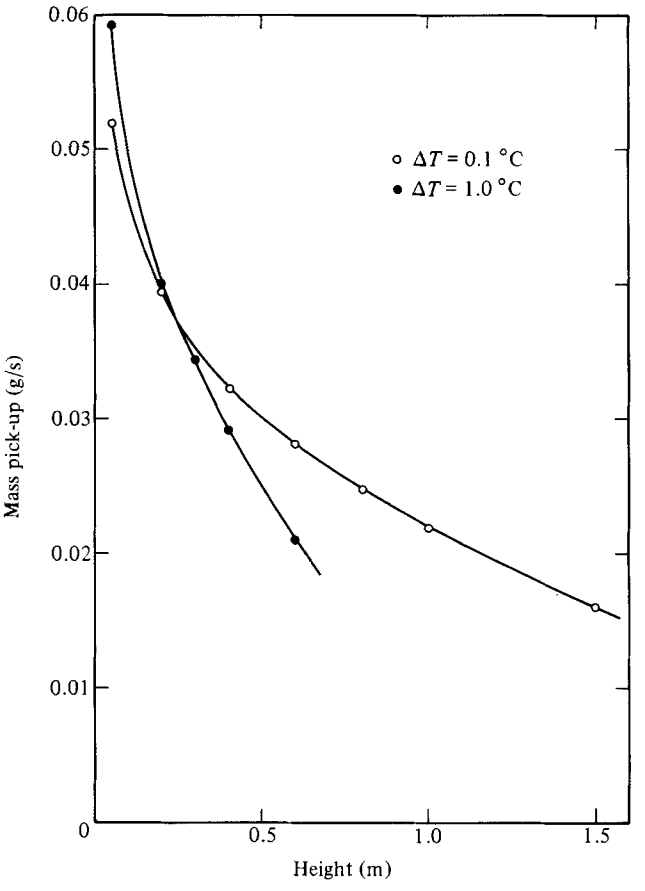


FIGURE 11. Computed mass pickup by evaporation and removal by forced ventilation as a function of suction height above the slot bottom for two different amounts of stable stratification.

(40 ft) long containers and with eleven intercontainer slots 0.1 m wide. The container width was 2.36 m, giving slot spacing of 2.46 m. The air temperature near the bottom of the hold was taken as 10 °C. Dimensional mass evaporation rates are based on vapour pressure and diffusivity data for heptane. Calculations for numerous other fuels have been made by Sealand Corporation (using a slightly less general model) and are reported elsewhere (von Iperen 1979).

Calculations were made for various locations of a single suction pipe, for several air-flow rates and several stable-stratification temperatures. The effect of varying the height of the suction above the tank top is shown in figure 11 for a suction on the centreline of an idealized ship. Raising the suction from 0.05 m above the tank top to 1.5 m is seen to decrease the evaporation rate by a factor of 3.25 for a stable stratification of 0.1 °C over the hold height of 20 m. Since the evaporation rate varies as flow to the one-third power, to remove liquid with the suction at 1.5 m at the same rate as with it at 0.05 m the flow would have to be somewhat more than 34 times as great for the 1.5 m height ($3.25^3$). For a 1 °C stable stratification this effect of suction height is seen to be very much more pronounced.

Moving the suction laterally at constant height has comparatively little effect. This is illustrated in figure 12, which shows the dimensionless mass pick-up for two suction

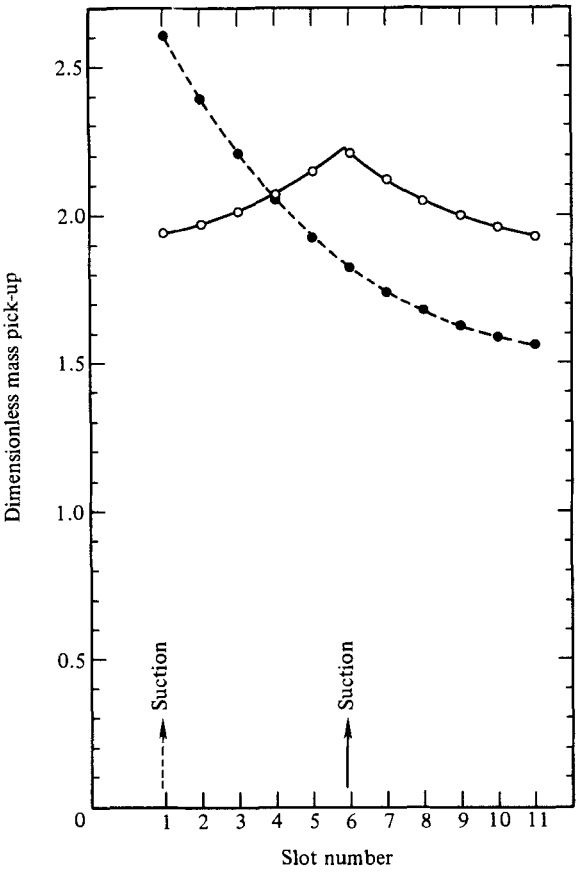


FIGURE 12. Dimensionless mass pickup as a function of slot number for a hold containing 11 slots (10 stacks of containers) for two forced ventilation suction locations: solid line, suction on hold centreline; dotted line, suction at the outboard corner of the hold.

locations, one on the centreline and the other near one side of the ship. However, since this calculation fails to account for the interference to transverse flow occasioned by the vertical framing of the bulkhead, these results should be viewed with caution. Figure 13(*a*) shows the calculated pressure at the open ends of a pair of slots, one on the hold centerline (solid line), the other the last slot outboard (dots). Pressures for two suction heights are shown: 0.05 m (figure 13*a*) and 0.6 m (figure 13*b*). Note that, except for a region of about 0.2 dimensionless units around the height of the suction, the pressures are essentially the same for the two slot locations at a given suction height. Since the slot flow is determined primarily by the gradient of the pressure at $y = 0$, little difference in the slot flows should be expected. This is reflected in the data presented in figure 12. Note also the effect on the pressures below the suction of raising it, i.e. compare in figures 13(*a*, *b*) the pressure behaviour below the pressure 'spike'. In figure 13(*b*) the pressure gradient is small between the tank top, $y = 0$, and a dimensionless height of about 0.1 (dimensional height 0.2 m). The very small pressure gradient at $y = 0$ results in little flow adjacent to the tank top and little scavenging of the flammable vapours. This accounts for the behaviour shown in figure 11 of mass-removal rate with suction height.

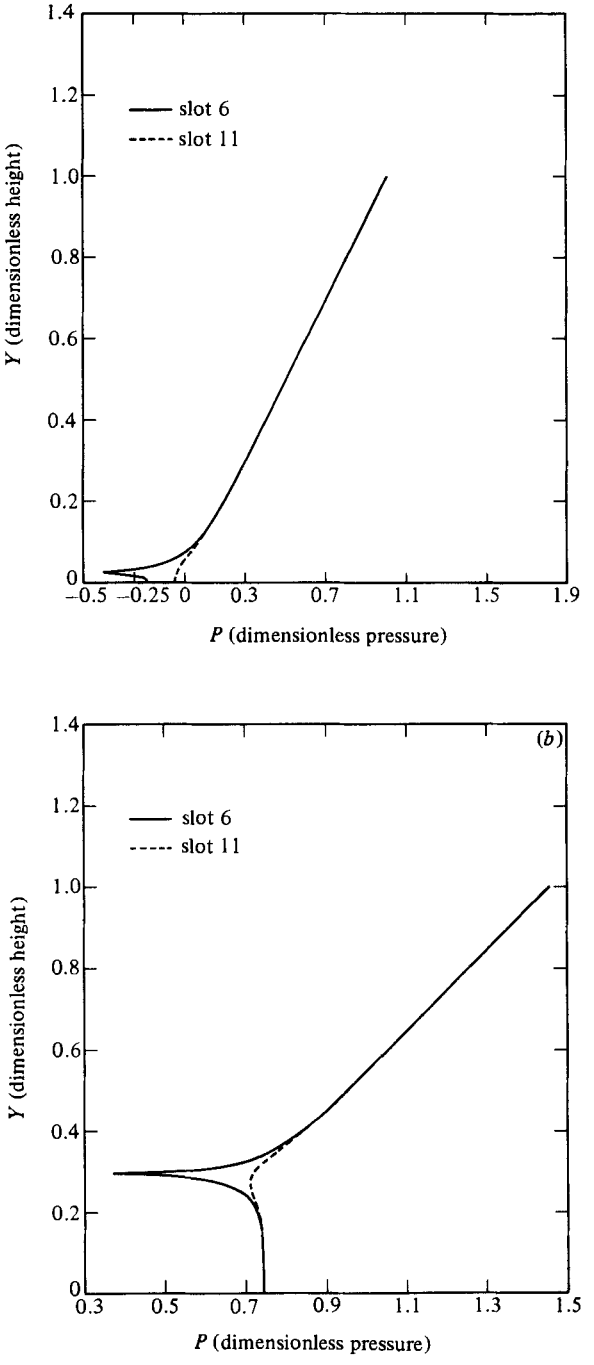


FIGURE 13. Dimensionless pressure as a function of dimensionless height stable stratification 0.1 °C over height of hold: (*a*) physical height of suction 0.05 m, dimensionless height 0.025; (*b*) Physical height of suction 0.60 m, dimensionless height 0.294.

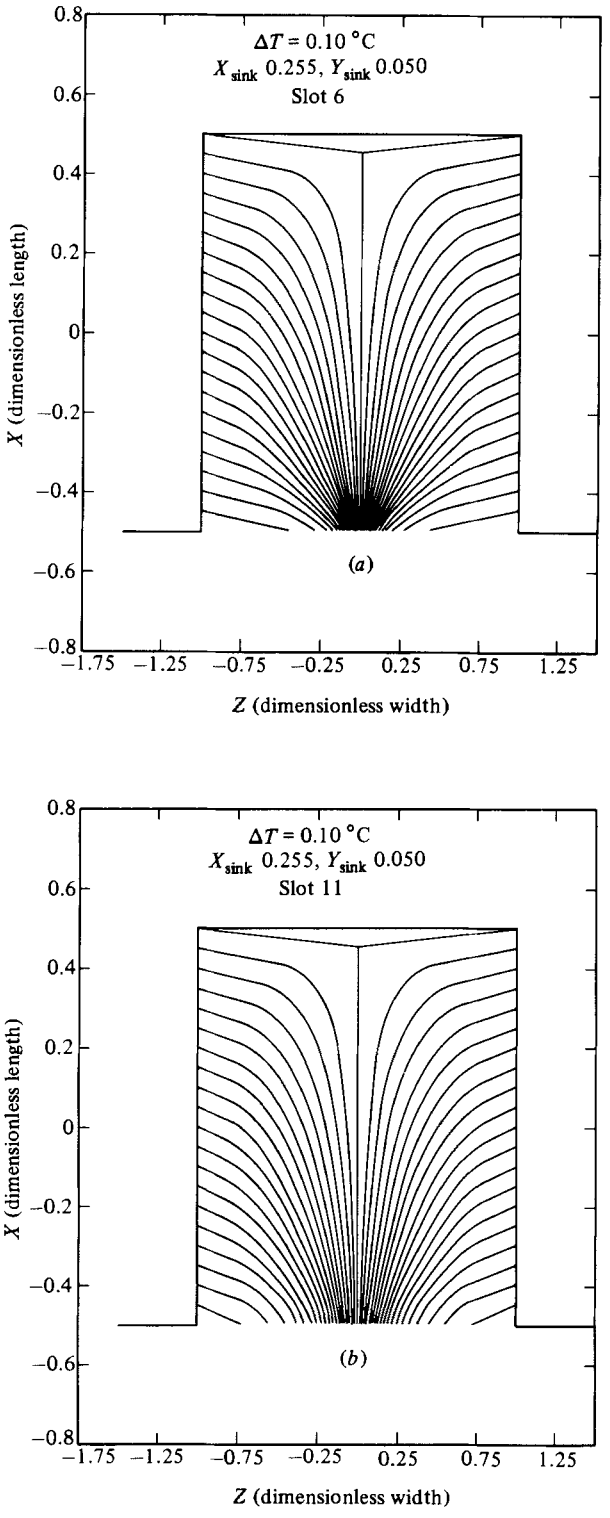


FIGURE 14. Slot bottom boundary-layer streamlines corresponding to the pressures shown in figure 13(*a*): (*a*) streamlines for slot at centre (nearest suction); (*b*) streamlines for slot at hold side (furthest from suction).

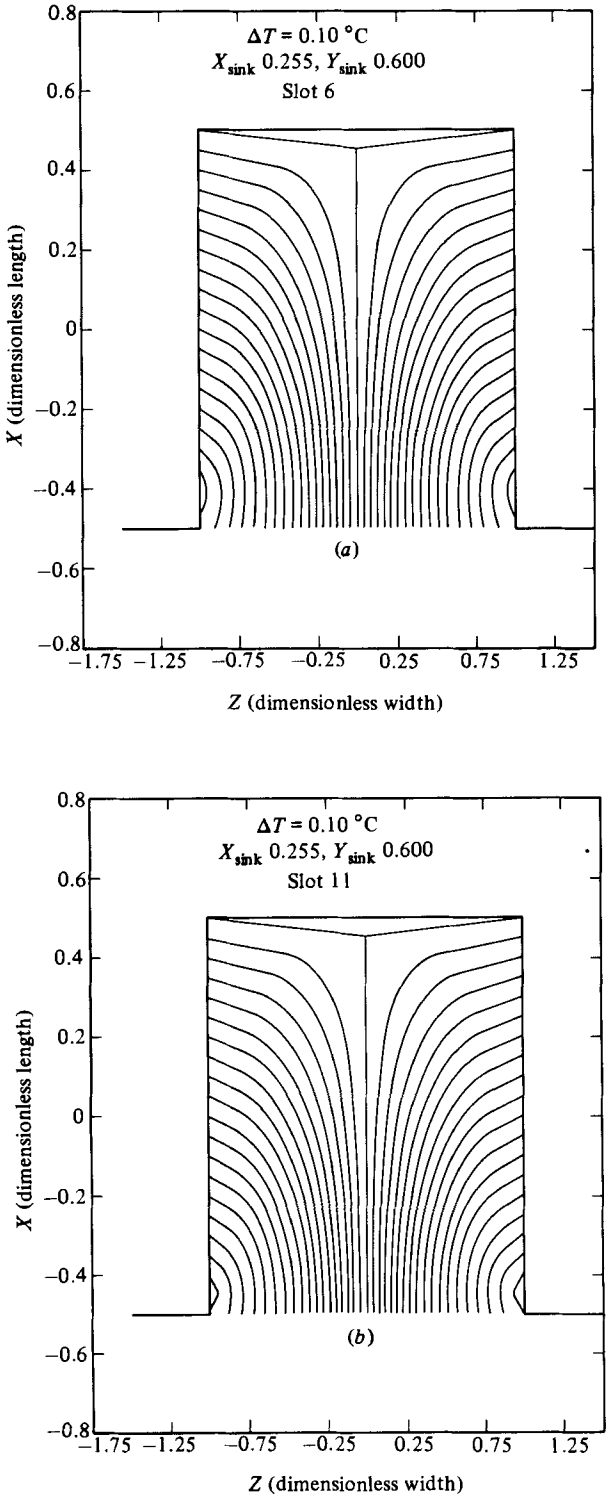


FIGURE 15. Slot bottom boundary-layer streamlines corresponding to the pressures shown in figure 13(*b*): (*a*) streamlines for slot at centreline (nearest suction); (*b*) streamlines for slot at hold side (furthest from suction).

Streamlines corresponding to the two sets of paired pressure distributions (figures 13$a, b$) are shown in figures 14$(a, b)$ and 15$(a, b)$. In these the transverse scale has been expanded about 100 times relative to the longitudinal scale. The drawings should be very attenuated in width to represent the geometry properly, but, if so presented, would be unreadable. The first pair (figure 14) show the streamlines for the boundary-layer flow at the bottom of the slots for the suction only 0.05 m above the tank top. A thin layer of gas flows down the sides of the containers and spreads out over the slot bottom – streamlines originating at the sides. It turns and flows along the slot bottom toward the open end of the slot. For the slot closest to the suction the streamlines are strongly bunched in the centre of the slot. For the slot farthest away from the suction the behaviour is similar but the bunching of the streamlines near the centreline of the slot is less pronounced. As the suction is raised there is quite a noticeable change in the flow which becomes more marked as the suction is raised. This change is seen by comparing figures 14$(a)$ and 15$(a)$. With the suction raised, not all the flow leaves the slot along its bottom surface. Some returns to the container sides and flows up, turning toward the main void as it approaches the height of the suction. By the same score, not all the flow descends in the thermal boundary layer next to the container sides to the slot bottom, although it does toward the rear of the slot. Some of the flow near the opening into the void turns as it approaches the height of the suction and exits directly. This flow is shown schematically in figure 10. Note that flow descending all the way to the tank top has actually been overcooled. In the stably stratified situation pertaining, it must be warmed again in order to rise to the height of the suction. To gain heat it must pass close to either the walls of the main void or of the slot. Obviously, for the suction raised well above the tank top, some of the air finds it easier to seek the slot sidewall rather than the main void walls. This flow behaviour was found through the numerical calculation. Although it is completely plausible, it was not anticipated. As the suction is further raised the flow along the slot bottom becomes still weaker and the tendency to return to the wall decreases. It has almost completely disappeared with the suction at 1 m.

The effect of increasing the stable thermal stratification is seen by comparing figures 13$(a)$ and 16. Note the different ordinate scales of the pressure plots. In figure 13$(a)$ the temperature difference over the 20 m hold height is 0.1 °C, while in figure 16 it is 1.0 °C. The dimensional suction heights are the same but, owing to the greater thermal stratification, the dimensionless height at $\Delta T = 1.0$ °C is greater. In general, the effect of increasing $\Delta T$ is to compress the vertical scale of the flow. With a higher $\Delta T$ the same vertical suction height appears to the flow as futher from the tank top.

Increasing the stable temperature stratification accentuates the flow effects as shown in figures 14 and 15. The flow in the slot closest to the suction bunches strongly but then spreads rapidly as the mouth of the slot is approached.

The main computed results for a given hold configuration and temperature stratification are expressed in dimensionless form for a nominal temperature of 10 °C. To obtain dimensional output the ventilation flow and spill-liquid partial pressure and diffusivity are needed. Some vapour pressure data as a function of temperature can be found in Hodgman (1943), and typically the logarithm of the vapour pressure is nearly linear with $1/T$ as shown for heptane in figure 2. Although the theory for vapour pressure is very well developed (Sommerfield 1956), a much simpler semi-empirical approach, Antoine's formula, is found in Hirata, Oke and Nagahame (1975):

$$\log p = A + \frac{B}{C+T},$$

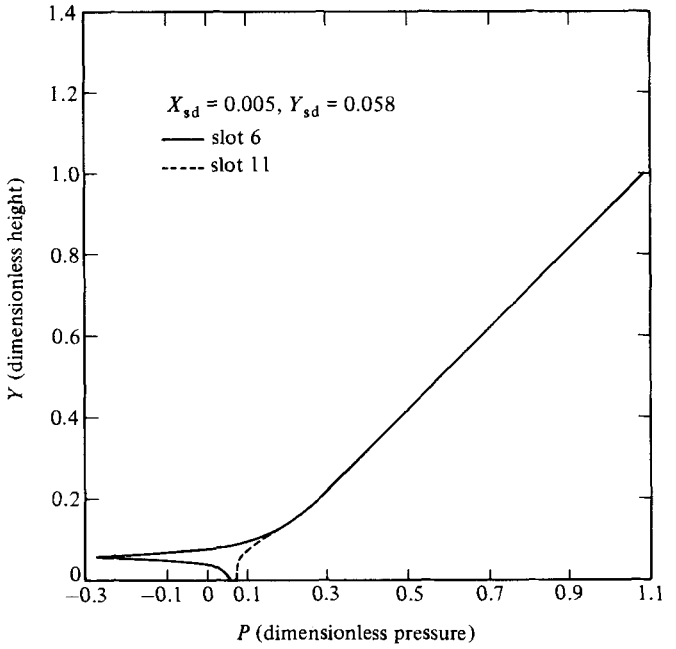


FIGURE 16. Dimensionless pressure as a function of dimensionless height, stable stratification 1.0 °C over height of hold.

where $p$ is the partial pressure, $T$ temperature and $A$, $B$, $C$ constants unique to the particular chemical. Further, since Hirata *et al.* give values for these constants for a large number of chemicals, their approach was used. Diffusivity data was corrected for temperature using the empirical relation given in Eckart (1963).

It is clear from figure 2 that the equilibrium vapour concentration is a strong function of temperature. The numerical calculation obtains the concentration for the input value of slot bottom temperature. However, the flow, which depends strongly on the differential stratification temperature, but only weakly on average ambient temperature, is computed using a nominal ambient.

## 9. Conclusions

One of the more interesting aspects of this study of a significant hazard to shipping was the almost total lack of previous scientific research at the time the initial decision of the International Maritime Consultative Organization relative to containership ventilation was made. Our limited study revealed many unanswered questions about fluid flow and heat and mass transfer in the context of maritime safety. It shed some light on one particular situation – the ventilation of a stably stratified containership hold. Many assumptions had to be made: when a surface temperature was needed, we assumed it was known; when geometric simplifications had to be made, it was assumed that associated complicated flow phenomena were not present. Despite these simplifications and idealizations, the work reported here is, to the best of our knowledge, the only analysis in existence that attempts to study the efficiency of ventilation in a realistic hold geometry and thermal environment.

Although much more detailed research should be done on a variety of specific

points, we believe that some important conclusions can be drawn from our study and that these conclusions will stand the test of time.

(1) In a stably stratified containership hold almost all the extracting capability of a ventilation system will be concentrated at the vertical level of the suction.

(2) In order to extract any significant amount of spilled material, it is essential to place the suction as close to the hold bottom as is feasible.

(3) With few exceptions, the natural tendency of vapours from spilled liquids will be to concentrate near the hold bottom. Therefore it is not efficient to try to design the ventilation system so as to mix the gas throughout the hold.

(4) Ventilation expressed simply as air changes per hour (for some arbitrary hold loading condition – empty or full) is a poor measure of performance. The performance will be sensitive to the thermal environment, degree of stratification and spacing between containers.

(5) The lack of the ability to analyse the thermal environment of a containership hold is a major impediment to systematic study of hold ventilation. There is important need for research in this area.

This work was sponsored by the U.S. Coast Guard. Sealand Corporation's cooperation was also important to the formulation of the problem and conduct of this work.

## REFERENCES

ABRAMOWITZ, M. & STEGUN, I. A. 1964 *Handbook of Mathematical Functions*. U.S. Natl Bur. Stand., U.S. Govt Printing Office.

BATCHELOR, G. K. 1967 *An Introduction to Fluid Dynamics*. Cambridge University Press.

BAUM, H. & ROCKETT, J. A. 1983 An investigation of the forced ventilation in containership holds. *NBSIR* 83-2665. U.S. Natl Bur. Stand.

BIRIKH, R. V., GERSHUNI, G. Z., ZHUKHOVITSKII, E. M. & RUDAKOV, R. N. 1969 Stability of the steady convective motion of a fluid with a longitudinal temperature gradient. *J. Appl. Maths Mech.* **33**, 937.

CARRIER, G. F. 1965 Analytical approximation techniques in applied mathematics. *J. SIAM* **13**, 68.

ECKART, H. R. G. 1963 *Introduction to Heat and Mass Transfer*. McGraw-Hill.

ELDER, J. W. 1965 Laminar free convection in a vertical slot. *J. Fluid Mech.* **23**, 77.

GILL, A. E. 1966 The boundary layer regime for convection in a rectangular cavity. *J. Fluid Mech.* **26**, 513.

HIRATA, H., OKE, S. & NAGAHAME, K. 1975 *Computer Aided Data Book of Vapor–Liquid Equilibrium*. Kodanska/Elsevier.

HODGMAN, C. D. 1943 *Handbook of Chemistry and Physics*, 27th edn. Chemical Rubber Publishing Co.

LEWIS, B. & VON ELBE, G. 1961 *Combustion, Flames and Explosion of Gases*. Academic.

LIGHTHILL, M. J. 1950 Contributions to the theory of heat transfer through a laminar boundary layer. *Proc. R. Soc. Lond.* A **202**, 359.

PRANDTL, L. 1952 *Essentials of Fluid Dynamics*. Blackie.

SCHLICHTING, H. 1955 *Boundary Layer Theory*. McGraw-Hill.

SOMMERFIELD, A. 1956 *Thermodynamics and Statistical Mechanics*, Academic.

TURNER, J. S. 1973 *Buoyancy Effects in Fluids*. Cambridge University Press.

VON IPEREN, W. H. P. 1979 A study of ventilation of containership holds for carriage of flammable liquids. Sea–Land Service, Inc., P.O. Box 1050, Elizabeth, NJ 07207.